Journal Pre-proofs

Generation of virtual geometric domains for woven textile composites

A.I. Akpoyomare, M.I. Okereke, M.S. Bingley

PII: S0263-8223(19)32473-0
DOI: https://doi.org/10.1016/j.compstruct.2019.111624
Reference: COST 111624

To appear in: *Composite Structures*

Received Date: 29 June 2019
Accepted Date: 29 October 2019

Please cite this article as: Akpoyomare, A.I., Okereke, M.I., Bingley, M.S., Generation of virtual geometric domains for woven textile composites, *Composite Structures* (2019), doi: https://doi.org/10.1016/j.compstruct.2019.111624

Generation of virtual geometric domains for woven textile composites

A. I. Akpoyomare[a,*], M. I. Okereke[a], M. S. Bingley[a]

[a] *Department of Engineering Science, Faculty of Engineering and Science, University of Greenwich, Kent, ME4 4TB, UK*

Abstract

The definition of an appropriate geometric domain is a prerequisite for performing virtual thermo-mechanical analyses on materials. Most of the current methods for generating virtual geometric domains for textile composites rely on complex equations conjured from the machining/manufacturing of the textiles; consequently, an intuitive method for developing a variety of virtual geometric domains for woven textile composites is desirable. The literature describes several techniques for generating geometric models for textile composites using advanced energy minimisation principles and computational imaging tools, but these techniques require specialist equipment, for deducing necessary empirical data, and heuristics to obtain acceptable results. This communication proposes a method for generating virtual geometric models using simple geometric metrics from the topology of the desired woven textiles. We describe and implement a geometric modelling algorithm for generating woven textile composites and show that the proposed technique yields geometric models with comparable characteristics to actual textile fabrics. Due to its modular structure, the proposed algorithm can be readily implemented on any programming platform and adapted to generate bespoke woven textile fabrics. This has been demonstrated by generating CAD models of woven textiles which can be adopted in any pre-processing tool for subsequent analysis in a finite element scheme.

Keywords: Textile composites, Geometric modelling, Meso scale, Virtual domains, Yarns, Cross-sectional shape functions

1. Introduction

Defining an appropriate virtual geometric domain is the cornerstone of any virtual characterisation test [1]. This step is important for heterogeneous materials such as composites because the spatial morphology of their constituents determine their mechanical properties [2, 3]. A vast majority of publications on the generation of virtual geometric domains for composites are on traditional composites such as unidirectional composites [4], particulate composites [5], and short fibre composites [6]. However, in comparison to

*Corresponding author
Email address: a.akpoyomare@gre.ac.uk (A. I. Akpoyomare)

publications on the aforementioned traditional composite materials, publications covering more complex composites such as advanced engineering textile composites are fewer. This shortage stems from the onerous challenges involved in generating computational replicas of textile composites [7]. Additionally, it is even more difficult to develop a single unified algorithm to generate geometric domains for different sub-classes of textile composites (i.e. braided, warp-knitted, woven). Therefore, algorithms for geometric model generation of textile composites focus on specific sub-classes and variants of textile composites: warp-knitted [8], braided [9], 2D woven [10], 3D woven [11] etc. However, these algorithms either require first-hand experience of the machining operation required to produce the textile, or rely on niche specialist equipment and skills [12, 13].

Geometric models of textiles may either explicitly model the fibres within each yarn (*micro-mechanical geometric models*), or approximate the geometry of a yarn as a solid volume (*meso-mechanical geometric models*). Wang and Sun [14] developed a numerical technique for generating micro-mechanical geometric models of textiles using so-called *digital elements*. Several authors [15, 16] extended this technique by modelling individual yarns as bundles of digital fibres, typically comprising tens of fibres. Durville [17, 18] also proposed a similar approach using beams to represent each fibre within yarns, whilst representing an entire yarn as a bundle of beams. These methods are completely general, thus, they can be easily used to represent any class of textile and have been used to perform elastic [17] and impact-related [16] constitutive analyses of dry fabrics. However, the veracity of these methods has not been thoroughly validated and scepticisms remain regarding the choice of tens of fibres incorporated in yarns, in contrast to the physically obtainable thousands of fibres within yarns [19]. More important, finite element (FE) meshing of such models is envisaged to pose onerous challenges resulting from minuscule, yet intricate, matrix pockets created between individual fibres within yarns. Thus, in textile composite analyses, meso-mechanical models are more commonplace because of their practical convenience, versatility, and their lower computational demands, in comparison to micro-mechanical models.

Meso-mechanical geometric modelling of textiles typically comprises three major stages (1) fabric topological description, (2) yarn geometric description, and (3) textile volume description. Fabric topological description is defined at the outset during manufacturing: therefore, the taxonomy of a fabric describes its innate topology. A yarn's geometric description involves the definition of its volume which comprises the specification of its trajectory as well as localised cross-sectional areas at various loci along its trajectory. Finally, A textile's volume is an ensemble of yarns which represents the spatial placement, orientation and interaction of individual yarns which collectively comprise the fabric under consideration. Therefore, the primary consideration for generating virtual domains for textile composites involves the geometric description of yarns. Four principal methods for describing yarn paths are commonly used in the literature: (1) geometric methods, (2) mechanical methods, (3) mixed geometric-mechanical methods, and (4) phenomenological methods.

Geometric methods determine trajectories of yarns strictly from geometric arguments of a fabric's topology. This method was pioneered by the seminal work of Peirce [20] who used a combination of circular/elliptical arcs and straight line segments to describe the trajectory of yarns in plain weave fabrics. Kemp [21] later refined Peirce's method by considering more flattened cross-sections of yarns. Another variant of geometric yarn path modelling is the so-called *saw-tooth model.* in which yarns are considered to have straight, possibly undulating, segments only [22, 9, 9, 8, 23]. Mechanical yarn path descriptors determine trajectories of yarns primarily from the mechanical properties of yarns; these properties include yarn bending rigidity, yarn compressibility (flattening), twisting, and inter-yarn friction [24, 25, 12, 26]. The constitutive physics of such models uses energy minimisation principles. An advantage of mechanical yarn path descriptors is their ability to predict a variety of geometric features unachievable using geometric yarn path descriptors: yarn skewness [24] (side deflection), localised yarn flattening (compaction) [27, 28], fabric nesting [29, 30] etc. Nevertheless, the minimum energy principle problem is ill-posed in cases where yarns are loosely supported within a fabric. This leads to poor, or lack of, convergence of the energy minimisation process [26, 7]. Additionally, the non-conservative mechanical nature of textiles also invokes convergence challenges. Thus, heuristic techniques are mandatory to yield acceptable solutions [31]. Mixed geometric-mechanical yarn path descriptors, use a combination of geometric and mechanical yarn path description techniques. This technique is identical to Peirce's method described earlier. However, instead of using straight line segments at non-crossover regions (as in Peirce's method), an approximate solution to an energy minimisation problem is invoked within this region [31], using polynomials. Lastly, phenomenological yarn path descriptors define yarn paths directly from experimental observations of fabric samples using optical scanning, optical microscopy, confocal microscopy, optical coherence tomography and x-ray micro-tomography techniques [32, 19]. The main advantage of this technique is its ability to reproduce the exact fabric geometry. However, this technique is devoid of any predictive aspect and it requires specialist instrument, expertise and significant resources to implement.

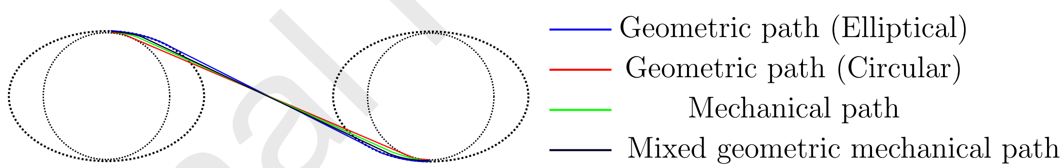

Figure 1: Schematic showing comparisons between various yarn path descriptors [33]. Note that the circular and elliptical cross-sections are included for visualisation purposes only.

Lomov and Robitaille [31] analysed and compared yarn paths generated using Peirce's geometric descriptors and advanced mechanical and mixed geometric-mechanical descriptors which use the energy minimisation principle. They concluded that all yarn path description methods yield similar results with negligible differences, especially when Peirce's modified elliptical method is adopted. A schematic of the comparison is shown in Figure 1. Therefore, they proposed that an ideal solution might be obtained by using a method which combines the advantages of these methods. Furthermore, Provatidis and Vassiliadis [22] investigated the performance of the aforementioned methods for generating virtual fabric geometric models. The authors concluded that Peirce's modified method yields the most representative description of textile fabrics. Recently, Hivet and Boisse [13, 34, 10] justified and validated this Peirce's modified geometric modelling method from extensive experimental analyses of twill weaves using micrographs and optical tomography.

A major problem with most virtual domains generated using simple geometric descriptors is the lack of correspondence between the intra-yarn fibre volume fraction, iy-V_f, and fabric thickness, H, in comparison to experimental data [35, 36, 37]. Furthermore, experimental evidence demonstrates that actual fabrics have flushed surfaces [37, 38], unlike common geometric models which have spurious matrix pockets at surfaces of fabrics [**?**] caused by overhanging warp-wise yarns. Thus, it is common practice to introduce excessive values for iy-V_f (i.e. $\geqslant 75\,\%$) [35], values which exceed experimental observations, in order to match the overall fibre volume fraction, o-V_f of fabrics. Conversely, models that attempt to maintain acceptable iy-V_f values typically suffer from excessive yarn flattening and inter yarn penetrations, features which are realistically inadmissible [37]. Therefore, a method which adopts the intuitive and simple geometric yarn Pierce-style descriptor as well as addressing its aforementioned common problems is desirable.

In this communication, we describe and implement a virtual geometric modelling algorithm particularly amenable to woven textiles, TextCompGen. We adopt a similar philosophy to Pierce, however, the geometric arguments are extended to consider relevant experimental features such as flushed fabrics surfaces, admissible intra-yarn fibre volume fraction and fabric thickness. Furthermore, robust definitions of local yarn cross-sectional shapes capable of describing a plethora of shapes are also implemented. Section 2 starts by delineating the nomenclature adopted in this work for describing typical woven fabrics. Subsequently, the spatial ordering of yarns in the in-plane and out-of-plane directions within woven fabrics are outlined. Section 3 describes specifics relating to the definition of individual yarn volumes within a fabric. Section 4 discusses the requisite input parameters for generating virtual textile geometric domains. introduces pertinent formulations required to determine the physical properties of generated textiles from TextCompGen. Finally, Section 6 demonstrates the applicability of TextCompGen by considering a numerical example of generating a through-thickness angle-interlock textile.

2. Textile architecture

The architecture of a textile is determined by its topology and the geometry of its constituent yarns. A textile's topology refers to the mutual interlacing patterns of yarns comprising the textile. This topology arises during fabrication of a textile, or in predictive cases, is pre-determined based on modelling requirements. Therefore, the topology of a textile can be described as a set of spatial orderings between individual yarns along in-plane and out-of-plane directions [39]. The geometry of yarns within a textile is determined by their paths/trajectories, which naturally arise from fabric topology, and local cross-sectional shapes and dimensions. Thus, generating virtual textile domains necessitates the formulation of schemes to define two principal things: (1) textile topology, and (2) yarn geometry.

2.1. Textile topology

Figure 2 shows the parameters used herein to define aspects of a woven textile in $\mathbb{R}^3$. All vectors are dimensional along X, Y and Z. Warp-wise (i.e., warp and binder) and weft-wise (i.e., weft) yarns extend the X and Y directions respectively. Yarns undulate along the Z direction.

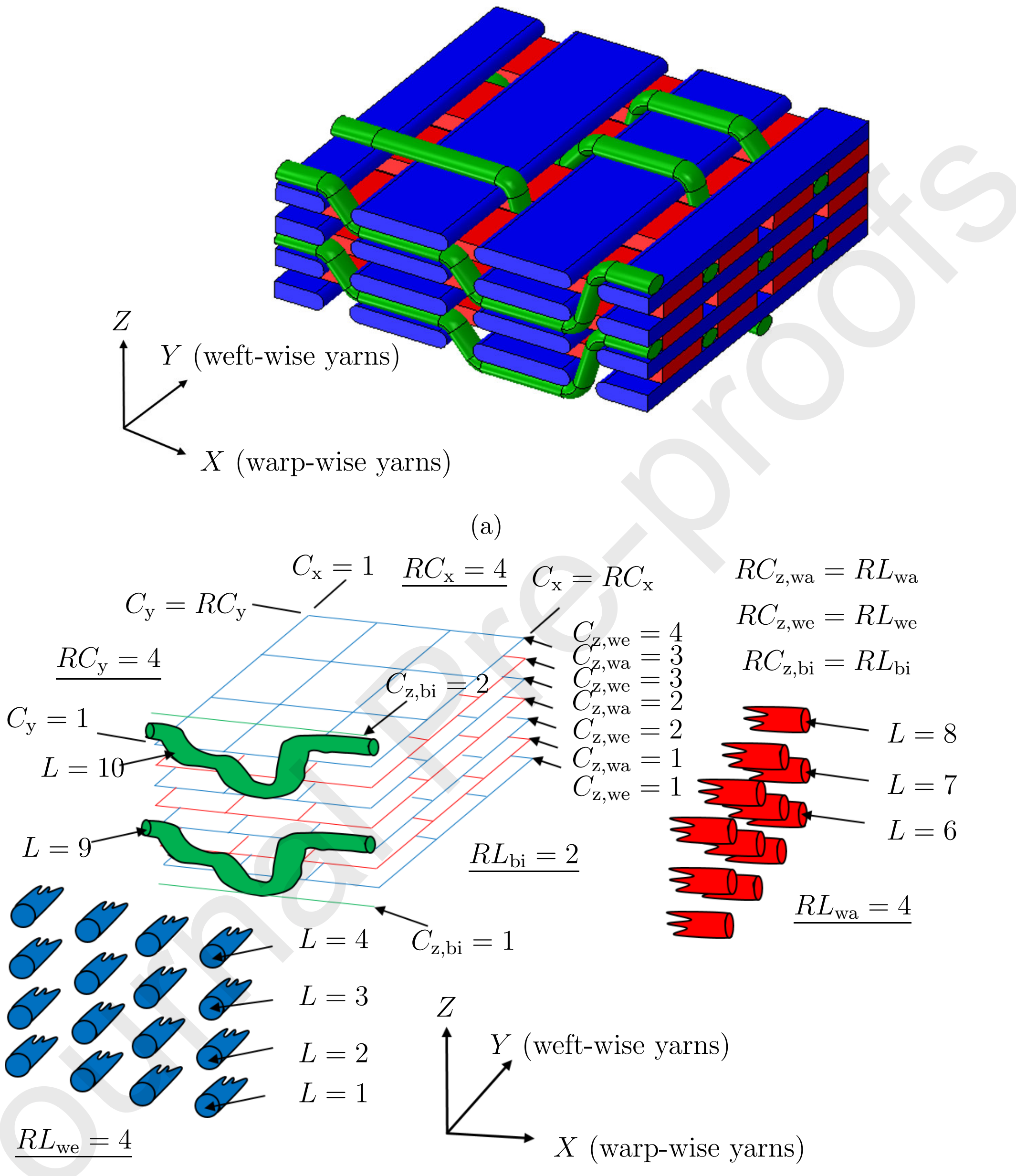

(a)

(b)

Figure 2: Schematic representation of the nomenclature used to define the topology of a typical woven fabric in $\mathbb{R}^3$: (a) typical sample of a multi-layered angle interlock woven fabric, and (b) schematic showing the nomenclature of representative parameters for defining the unit cell in $\mathbb{R}^3$.

2.1.1. Identification of crossover regions, yarn layers and yarns

Crossover regions are locations where yarns interlace within a fabric. These crossover regions are identified by projecting the centre trajectories of yarns comprising the textile on a plane parallel to the fabric's face (i.e. the XY plane). Each crossover region is identified by the sampling couple $\left(C_{\mathrm{x}}, C_{\mathrm{y}}\right)$, where

$$C_{\mathrm{x}} = 1, 2, \cdots, RC_{\mathrm{x}} \quad \text{and,} \tag{1a}$$
$$C_{\mathrm{y}} = 1, 2, \cdots, RC_{\mathrm{y}}. \tag{1b}$$

where C_{x} and C_{y} increase in the positive X and Y directions, and RC_{x} and RC_{y} represent the maximum number of weft-wise and warp-wise yarns in increasing positive X and Y axes, respectively.

The total number of layers corresponding to the warp, weft and binder yarns are denoted as $RL_{\mathrm{wa}}, RL_{\mathrm{we}},$ and RL_{bi}, respectively. Furthermore, any yarn layer within the textile is defined by the variable L. Each layer, L, within the textile is defined as

$$L = 1, 2, \cdots, RL_{\mathrm{we}}, \text{ for weft yarns;} \tag{2a}$$
$$L = \left(RL_{\mathrm{we}} + 2\right), \left(RL_{\mathrm{we}} + 3\right), \cdots, \left(RL_{\mathrm{we}} + RL_{\mathrm{wa}} + 1\right), \text{ for warp yarns; and} \tag{2b}$$
$$L = \left(RL_{\mathrm{wa}} + RL_{\mathrm{we}} + 2\right), \left(RL_{\mathrm{wa}} + RL_{\mathrm{we}} + 3\right), \cdots, \left(RL_{\mathrm{wa}} + RL_{\mathrm{we}} + RL_{\mathrm{bi}} + 1\right), \text{ for binder yarns;} \tag{2c}$$

Having defined the entire crossover regions and yarn layers within the textile, individual warp, weft and binder yarns are identified by the sampling couples (L, C_{x}), $\left(L, C_{\mathrm{y}}\right)$.

2.1.2. Out-of-plane yarn sequences

The mutual interlacing pattern of yarns in the out-of-plane direction is specified via a *weaving matrix*, $\mathbf{W}$, of warp-wise yarns. This weaving matrix, $\mathbf{W}$, has dimensions $RC_{\mathrm{y}} \times (RL_{\mathrm{wa}} + RL_{\mathrm{bi}})$. The number of rows, RC_{y}, corresponds to the number of projected warp-wise yarns along the Y axis whilst the number of columns, $(RL_{\mathrm{wa}} + RL_{\mathrm{bi}})$, corresponds to the sum of the total number of warp and binder yarn layers. Each term within $\mathbf{W}$ is a weaving vector, $\mathbf{WV}\left(C_{\mathrm{y}}, C_{\mathrm{z,wa}} + C_{\mathrm{z,bi}}\right)$, of dimension RC_{x}. Each term within each weaving vector represents the level identifier of the weft layer situated above the warp-wise yarn in its intersection at the C_{x}'th cross-over point, or $RL_{\mathrm{we}} + 1$, if the warp-wise yarn lies on the top surface of the fabric, or a boolean value of $\varnothing$ if no warp-wise yarn is present. Cases where no warp-wise yarn is present can occur when the number of binder yarn layers for a given C_{x}'th cross-over point is less than the number of warp yarn levels RL_{wa} as is depicted in Figure 2 for $C_{\mathrm{x}} = 1$ where $RL_{\mathrm{bi}} < RL_{\mathrm{wa}}$. The out-of-plane weaving structure of weft-wise yarns are implicitly obtained from $\mathbf{W}$ and a crimp interval vector discussed in Section 3.2.

2.1.3. In-plane yarn sequences and type

The in-plane dimensions of a fabric depend on the periodicity and separating pitch of the warp-wise and weft-wise yarns. The values of the pitch separating the centre lines of the warp-wise and weft-wise yarns are specified as distances between adjacent yarns along the positive direction of the X and Y axes respectively, for a given layer. These values are grouped in three weave pitch vectors: $\mathbf{WP}_{\mathrm{we}}$, $\mathbf{WP}_{\mathrm{wa}}$ and $\mathbf{WP}_{\mathrm{bi}}$ for weft, warp and binder yarns, respectively. The dimensions of $\mathbf{WP}_{\mathrm{we}}$. $\mathbf{WP}_{\mathrm{wa}}$ and $\mathbf{WP}_{\mathrm{bi}}$ are $RC_{\mathrm{x}} \times RC_{\mathrm{z,we}}$, $RC_{\mathrm{y}} \times RC_{\mathrm{z,wa}}$ and $RC_{\mathrm{y}} \times RC_{\mathrm{z,bi}}$, respectively. In cases where specific warp-wise yarns are absent along the RC_{y}'th co-ordinate, a boolean value of $\varnothing$ is assigned.

Each yarn within a fabric can be assigned a unique feature using reference numbers or IDs corresponding to a set of properties such as material type, density, cross-sectional shape etc. This information grouped in three yarn type vectors: $\mathbf{YT}_{\mathrm{we}}$, $\mathbf{YT}_{\mathrm{wa}}$ and $\mathbf{YT}_{\mathrm{bi}}$ for weft, warp and binder yarns, respectively. The dimensions of $\mathbf{YT}_{\mathrm{we}}$. $\mathbf{YT}_{\mathrm{wa}}$ and $\mathbf{YT}_{\mathrm{bi}}$ are $RC_{\mathrm{x}} \times RC_{\mathrm{z,we}}$, $RC_{\mathrm{y}} \times RC_{\mathrm{z,wa}}$ and $RC_{\mathrm{y}} \times RC_{\mathrm{z,bi}}$, respectively.

3. Yarn geometry

In order to define a yarn's geometry two important features must be described: (1) its local cross-section, and (2) its path/trajectory. These two salient features are described in more detail within the following sections.

3.1. Yarn cross-section

A yarn's cross section refers to a two-dimensional region in space that encloses all the constituent fibres comprising the yarn. This cross section is generally convex due to the requirement of enclosing a finite set of fibres with each yarn. Common two-dimensional shapes used to describe a yarn's cross section include, but may not be limited to, the following: circular, lenticular, rectangular, ellipse, racetrack and tow element [40]. In general, these primary shapes do not adequately describe the geometry of actual yarns. In this study, additional cross sectional shapes which are more representative than the ones listed above have been implemented [19]. These shapes include a *power-ellipse* and a *modified lenticular shape* based on the formalisms presented by previous researchers [41, 42, 20]. The pseudo-vector for all the cross sectional shapes described henceforth are denoted by the symbol, $\mathbf{C}$.

3.1.1. Ellipse

Ellipses are, arguably, the most common form of two-dimensional shapes used for yarn cross-section approximation. Given its height, h, and width, w, the parametric form of an ellipse is

$$C(u)_x = \frac{w}{2}\cos(2\pi u)\text{for } u \in [0,1]\,, \tag{3a}$$

$$C(u)_y = \frac{h}{2}\sin(2\pi u)\text{for } u \in [0,1]\,. \tag{3b}$$

Circles are degenerate forms of ellipses and thus can be obtained by specifying equal width and height in Equation (3). Figure 3 shows an example of an ellipse.

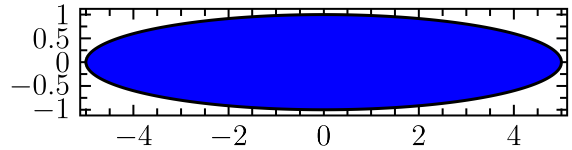

Figure 3: Sample of an elliptical cross section with aspect ratio, w/h, of 5.

3.1.2. Power ellipse

A power ellipse is a modified form of the classical ellipse described in Section 3.1.1. The difference is in the computation of the y co-ordinate which is ascribed a power index, n, to alter the generated shape of the governing equations. The power index may be described as a *shape parameter*. The resulting generated shape is rectangular with rounded edges when $n < 1$, or lenticular when $n > 2$ [42]. A parametrised power ellipse is given by

$$
\begin{aligned}
C(u)_x &= \frac{w}{2}\cos(2\pi u) \qquad\quad \text{for } u \in [0,1]\,,\\
C(u)_y &= \begin{cases} \dfrac{h}{2}\sin(2\pi u)^n & \text{for } u \in [0,0.5]\,,\\[2ex] \dfrac{-h}{2}\sin(2\pi u)^n & \text{for } u \in [0.5,1]\,, \end{cases}
\end{aligned} \tag{4}
$$

where w,h, and n, represent the width, height and shape parameter of the power ellipse. Several examples of power ellipses are shown in Figure 4.

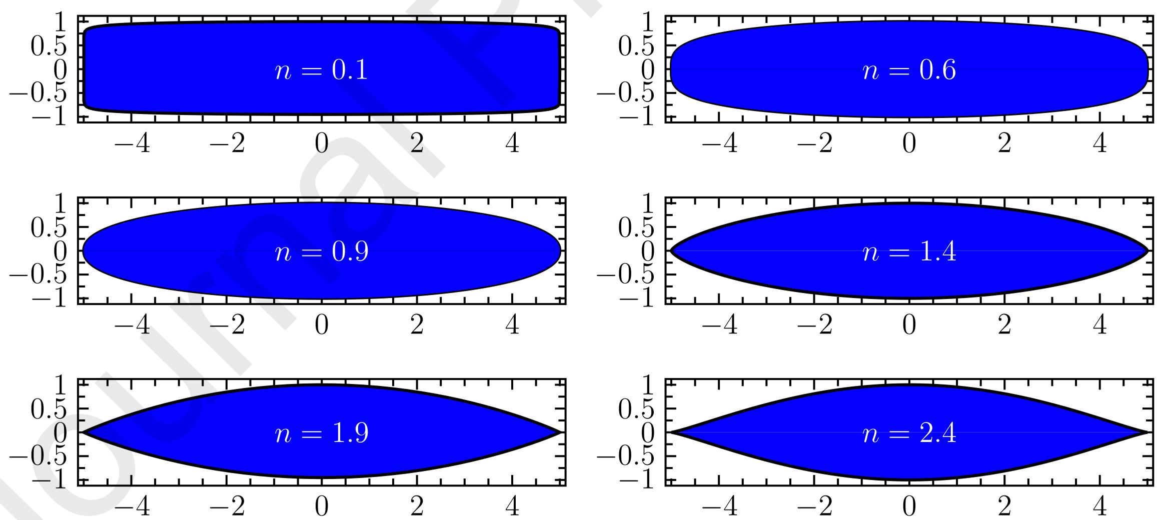

Figure 4: Schematic of power-ellipse cross section with different shape parameters and identical aspect ratios.

3.1.3. Lenticular

A lenticular shape defines the region of intersection between two circles, with equal or different geometric dimensions (i.e. diameter), when they are offset by a certain distance from a reference configuration. The lenticular region is given by three key geometric dimensions: its width, w; height, h; and distortion distance α. These, in turn, are characterised by the dimensions of each of the circles comprising the lenticular shape. The parametric form of a lenticular shape is

$$
\begin{aligned}
C(u)_x &= \begin{cases} \dfrac{d_1}{2}\sin(\psi) & \text{for } u \in [0, 0.5] \\ \dfrac{d_2}{2}\sin(\psi) & \text{for } u \in [0.5, 1] \end{cases} \\
C(u)_y &= \begin{cases} \dfrac{d_1}{2}\cos(\psi) + o_1 & \text{for } u \in [0, 0.5] \\ \dfrac{-d_2}{2}\cos(\psi) + o_2 & \text{for } u \in [0.5, 1] \end{cases}
\end{aligned}, \tag{5}
$$

where

$$
\begin{aligned}
d_1 &= \frac{w^2 + (h - 2\alpha)^2}{2(h - 2\alpha)}, \\
d_2 &= \frac{w^2 + (h + 2\alpha)^2}{2(h + 2\alpha)}, \\
o_1 &= \frac{-d_1 + h}{2}, \\
o_2 &= \frac{d_2 - h}{2},
\end{aligned}
$$

and

$$
\psi = \begin{cases} (1 - 4u)\sin^{-1}\left(\dfrac{w}{d_1}\right) & \text{for } u \in [0, 0.5] \\ (-3 + 4u)\sin^{-1}\left(\dfrac{w}{d_2}\right) & \text{for } u \in [0.5, 1] \end{cases}.
$$

The parameters, d_1, d_2, o_1 and o_2 refer to the radii and offset distances between the circles comprising the lenticular shape. Examples of different lenticular shapes are shown in Figure 5.

3.2. Yarn path

Recall that a yarn path can be defined as a series of infinitesimal line segments that collectively trace the trajectory of the centreline of any given yarn in $\mathbb{R}^3$, between two primary datum points: the start and end points of the yarn. Although these primary datum points specify terminal locations along a yarn's trajectory, generally, the path traversed at intermediate locations between these limits is arbitrary. This path is dependent on the mutual interaction between contacting yarns within the textile. Therefore, a generic way of defining an approximate yarn trajectory is necessary.

Geometric arguments represent a simple way of defining the trajectory of yarns within a textile without recourse to mechanical arguments such as yarn friction and compressibility [43]. Geometrically, the path of a weaving yarn is dictated by the local cross-sectional shape of adjacent yarns with which this weaving yarn contacts. Thus, the local cross-sectional shape of yarns and the mutual interaction between yarns (i.e., textile topology)

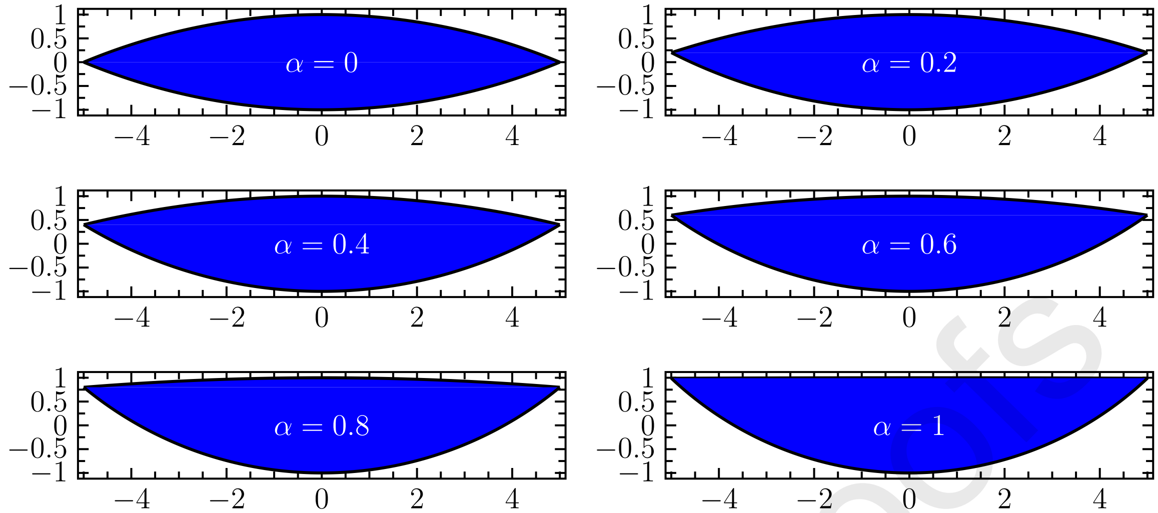

Figure 5: Schematic of lenticular cross-sectional shapes with different distortion parameters and the same aspect ratios.

provides a basis upon which the path of a yarn is described. In order to simplify the problem, the entire path of a yarn is divided into several segments called *crimp intervals* as shown in Figure 6. A crimp interval represents a yarn segment which extends between two in-plane crossover points. Over the first crimp interval for this warp-wise yarn, it interacts with the weft-wise yarns in layers $L_1^1 = 4$ and $L_1^2 = 4$, where the subscript represents the crimp interval's number and the superscript corresponds to the start and end index of the interval (i.e., 1 = left end and 2 = right end). This yarn sits above its supporting weft-wise yarn at the left end of the crimp interval (i.e., 1) and below its supporting weft-wise yarn on the right end of the crimp interval (i.e., 2). These support positions within this interval are represented as $P_1^1 = +$ and $P_1^2 = -$, respectively. The entire crimp interval data for this yarn is given by

$$\begin{array}{llll} L_1^1 = 5, & L_1^2 = 4, & P_1^1 = +, & P_1^1 = -; \\ L_2^1 = 4, & L_2^2 = 3, & P_1^1 = +, & P_1^1 = -; \\ L_3^1 = 3, & L_3^2 = 5, & P_3^1 = -, & P_3^1 = +. \end{array} \tag{6}$$

The data in Equation (6) can be obtained from the terms weaving vectors $\mathbf{W}\left(C_{\mathrm{y}}, C_{\mathrm{z,wa}}\right)$ contained within the weaving matrix of warp-wise yarns, $\mathbf{W}$, using the following algorithm:

$$\begin{array}{lll} \mathbf{WV}_i = \mathbf{WV}_{i+1} \Rightarrow & L_i^1 = L_i^2 = \min(\mathbf{WV}_i - 1, RL_{\mathrm{we}}), & P_i^1 = P_i^2 = \begin{cases} +, & \text{if } \mathbf{WV}_i < RL_{\mathrm{we}} \\ -, & \text{if } \mathbf{WV}_i = RL_{\mathrm{we}} \end{cases} ; \\ \mathbf{WV}_i < \mathbf{WV}_{i+1} \Rightarrow & L_i^1 = \mathbf{WV}_i, L_i^2 = \mathbf{WV}_{i+1} - 1, & P_i^1 = -, P_i^2 = +; \\ \mathbf{WV}_i > \mathbf{WV}_{i+1} \Rightarrow & L_i^1 = \mathbf{WV}_i - 1, L_i^2 = \mathbf{WV}_{i+1}, & P_i^1 = +, P_i^2 = -; \end{array} \tag{7}$$

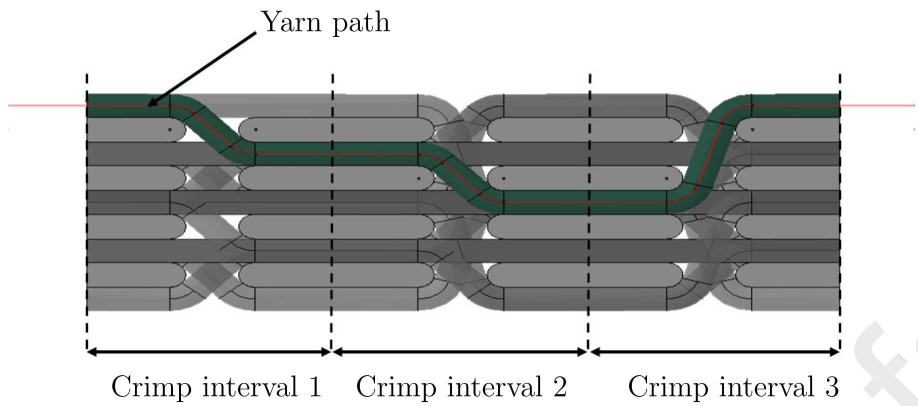

Figure 6: Illustration of crimp intervals along a yarn's path in a typical woven textile.

where $\mathbf{WV}_i$ corresponds to the i'th term in weaving vector for $i \in \{1, 2, \cdots, RC_\mathrm{x}\}$. The entire data set obtained by applying Equation (7) are stored in crimp interval matrices, $\mathbf{CI}_\mathrm{wa}$ and $\mathbf{CI}_\mathrm{bi}$, and support structure matrices, $\mathbf{SS}_\mathrm{wa}$ and $\mathbf{SS}_\mathrm{bi}$, for all the warp-wise yarns.

Similar descriptions for weft-wise yarns are obtained from crimp interval and support structure data of warp-wise yarns. For a weft-wise yarn given by the sampling couple $\left(C_\mathrm{x}, C_\mathrm{z,we}\right)$, the first warp-wise yarn with $L^1_{C_\mathrm{x}} = C_\mathrm{z,we}$ or $L^2_{C_\mathrm{x}} = C_\mathrm{z,we}$ (i.e., supported by weft-wise yarn C_x at layer $C_\mathrm{z,we}$) is obtained from the crimp interval parameters list, $\mathbf{CI}_\mathrm{wa}$ and $\mathbf{CI}_\mathrm{bi}$, this is the left end of the first crimp interval on the weft-wise yarn. The supporting warp-wise yarn layer and ID is thus found, with a weft-wise supporting structure's sign inverse to that of the warp-wise yarn. Subsequently, the next warp-wise yarn supported by the weft-wise yarn identified by the sampling couple $\left(C_\mathrm{x}, C_\mathrm{z,we}\right)$ is found; this is the right end of the first weft-wise crimp interval and the left end of the second crimp interval, and so on. The data obtained from these analyses are stored in crimp interval and support structure matrices, $\mathbf{CI}_\mathrm{we}$ and $\mathbf{SS}_\mathrm{we}$, respectively.

The actual path traversed by any yarn within a textile is given by its spatial conformation at non-crossover and crossover regions. All yarns are assumed to follow a straight path at non-crossover regions. At crossover regions, however, the path of any yarn follows an arbitrary curved shape identical to the local cross-sectional shape of its supporting yarn (i.e., the yarn it interacts with). This postulation yields a notion of *supporting contour*[24]. A supporting contour represents the local cross-sectional shape of a supporting yarn which is offset by a specific distance as shown in Figure 7. Typically, the offset distance is equal to half of the yarn height which the yarn supports. Consequently, each yarn path is specified in a piecewise manner. A prerequisite for defining the path of a yarn is that it must be, at least, C^1 continuous[1]. This continuity condition is necessary to prevent abrupt discontinuities and visible *creases* or *kinks* along a yarn, all of which are hallmarks of inherent damage and irregularities.

[1] Continuity is a term used to describe an unbroken curve within an interval. The order of continuity (i.e. C^n where $n \in \mathbb{Z}_{\geq 0}$) describes the degree to which a function's derivative is continuous over the same interval. For example, a function, f, having C^3 continuity means f''' is unbroken when evaluated over the given interval.

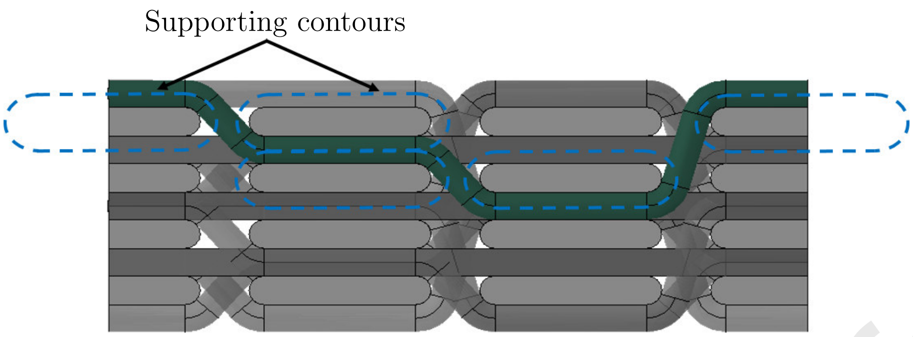

Figure 7: Depiction of supporting contours (dashed lines) used for determining the path of a yarn in a typical woven textile.

Given the preceding postulations about the spatial conformation of yarn paths at non-crossover and crossover regions, as well as its proposed piecewise representation, the path of an arbitrary yarn across one crimp interval, $\mathbf{S}_0(t)$, is given by

$$\mathbf{S}_0(t) = \begin{cases} \Omega^1\left(\rho_{\text{yarn}}, \mathbf{C}(u)\right) & \text{if } \begin{cases} u \in [0, u_{\text{crit}}]\,, \text{ or} \\ u \in [0.75, 0.75 + u_{\text{crit}}]\,, \end{cases} & \text{for } t \in [t_0, t_1] \\ (Au, \Delta_{\text{line}} Au + \alpha_{\text{line}}) & & \text{for } t \in [t_1, t_2] \\ \Omega^2\left(\rho_{\text{yarn}}, \mathbf{C}(u)\right) & \text{if } \begin{cases} u \in [0.75 - u_{\text{crit}}, 0.75]\,, \text{ or} \\ u \in [0.50, 0.50 + u_{\text{crit}}]\,, \end{cases} & \text{for } t \in [t_2, t_3] \end{cases} \tag{8}$$

where Ω^1 is the left end of the offset supporting contour, Ω^2 is the right end of the offset supporting contour, ρ is the specified offset distance, Δ_{line} is the gradient of the straight part of the yarn at a non-crossover region, α_{line} is the intercept of the straight line, and u_{crit} is the critical parameter value that guarantees at least C^1 continuity such that

$$\Delta_{\text{line}} \equiv \Omega^{1\prime}\big|_{\substack{u=u_{\text{crit}} \\ u=0.75+u_{\text{crit}}}} \equiv \Omega^{2\prime}\big|_{\substack{u=0.75-u_{\text{crit}} \\ u=0.50+u_{\text{crit}}}} \text{ and } \alpha_{\text{line}} \equiv \alpha_{\Omega^1}\big|_{\substack{u=u_{\text{crit}} \\ u=0.75+u_{\text{crit}}}} \equiv \alpha_{\Omega^2}\big|_{\substack{u=0.75-u_{\text{crit}} \\ u=0.50+u_{\text{crit}}}} \tag{9}$$

where $\Omega^{1\prime}$ represents the derivative of the offset supporting contour on the left end of the crimp interval, $\Omega^{2\prime}$ represents the derivative of the offset supporting contour on the right end of the crimp interval, and α_{Ω^κ} for $\kappa \in \{1, 2\}$ represents the intercept of a straight line which is tangential to the given point on the offset supporting contour being evaluated. In practice, evaluating Equations (8) and (9) is challenging therefore, a numerical scheme for obtaining a solution was devised as shown schematically in Figure 8. Equation (8) defines the path of yarn across one crimp interval; thus, the expression for the full path of a yarn across multiple crimp intervals, $\mathbf{S}(t)$, is given by

$$\mathbf{S}(t) = \begin{cases} \mathbf{S}_0(t) & \text{for } t \in [t_0, t_3] \\ \mathbf{S}_1(t) & \text{for } t \in [t_3, t_6] \\ \vdots & \\ \mathbf{S}_n(t) & \text{for } t \in [t_{n+2}, t_{n+5}] \end{cases} . \tag{10}$$

where normalisations are introduced such that $t_0 =$ and $t_{n+5} = 1$.

3.3. Yarn volumetric description

Methods for describing yarn paths and cross sections were presented in Sections 3.1 and 3.2, but a scheme of unifying these two entities is required to completely define any yarn. In general, a yarn's path within a textile is arbitrary; therefore, the base cross section defined for any given yarn has to conform to the local orientation of the yarn as its path is traversed.

Consider two sets of orthonormal right-handed basis, $\{\mathbf{N}, \mathbf{B}, \mathbf{T}\}$ and $\{\mathbf{X}, \mathbf{Y}, \mathbf{Z}\}$; the $\{\mathbf{N}, \mathbf{B}, \mathbf{T}\}$ basis refers to the *local reference frame* of a yarn, where $\mathbf{N}$ is the normal axis, $\mathbf{B}$ is the bi-normal axis and $\mathbf{T}$ is the tangential axis. Similarly, the $\{\mathbf{X}, \mathbf{Y}, \mathbf{Z}\}$ basis refers to the *global reference frame* of the entire textile. In principle, the components of the local reference frame are to a local space what the corresponding components of the global reference frame are to global space (i.e., $\mathbf{N}$ is similar to $\mathbf{X}$ and so on). Since the cross section defined for a yarn has to conform to the local orientation of the yarn, the cross-section, therefore, has to be rigidly affixed to the $\mathbf{NB}$ plane of the local reference frame and the $\{\mathbf{N}, \mathbf{B}, \mathbf{T}\}$ basis has to traverse the yarn. Consequently, the cross section of a yarn is always normal to a yarn path's local tangent. Figure 9 shows a schematic of a cross section affixed to the $\mathbf{NB}$ plane of the $\{\mathbf{N}, \mathbf{B}, \mathbf{T}\}$ basis.

The FrenetSerret formulas [44, 45] define the local orthonormal basis of any continuously differentiable curve in $\mathbb{R}$. Given a parametric differentiable curve, $\mathbf{S}(t)$, the formulas that define the tangential, normal and bi-normal basis vectors are given by

$$\hat{\mathbf{T}}(t) = \frac{\mathbf{S}'(t)}{|\mathbf{S}'(t)|}, \tag{11a}$$

$$\hat{\mathbf{N}}(t) = \frac{\mathbf{T}'(t)}{|\mathbf{T}'(t)|}, \text{ and} \tag{11b}$$

$$\hat{\mathbf{B}}(t) = \hat{\mathbf{N}}(t) \times \hat{\mathbf{T}}(t). \tag{11c}$$

For curves without curvature, Equation (11b) and, consequently, Equation (11c) are not defined. Therefore, alternative methods for deriving the normal and bi-normal basis vectors are required when Equation (11b) = 0 (i.e., when $\mathbf{T}'(t) = 0$). To achieve this, a so-called up vector, $\mathbf{U}$, is defined. Once the up vector is defined, the normal vector is given by

$$\hat{\mathbf{N}}(t) = \frac{\mathbf{U} \times \mathbf{T}(t)}{|\mathbf{U} \times \mathbf{T}(t)|}, \tag{12}$$

and Equation (11c) can be used subsequently to define the bi-normal basis vector. The definition of the up-vector is arbitrary; it may be regarded as a vector that points vertically upwards in the plane defining the local tangent to the curve. For example, a non-vertical curve along the $\mathbf{YZ}$ plane, with $\mathbf{Z}$ representing the elevation of the curve, may have an up-vector defined as $[0, 0, 1]$. As implied in the preceding statement, this definition works well for local yarn tangents which are not parallel to the up-vector, as parallelism between both vectors results in a zero normal vector (i.e. $\mathbf{U} \times \mathbf{T}'(t) = 0$). This exception will be prevalent for local yarn paths with vertical orientation such as

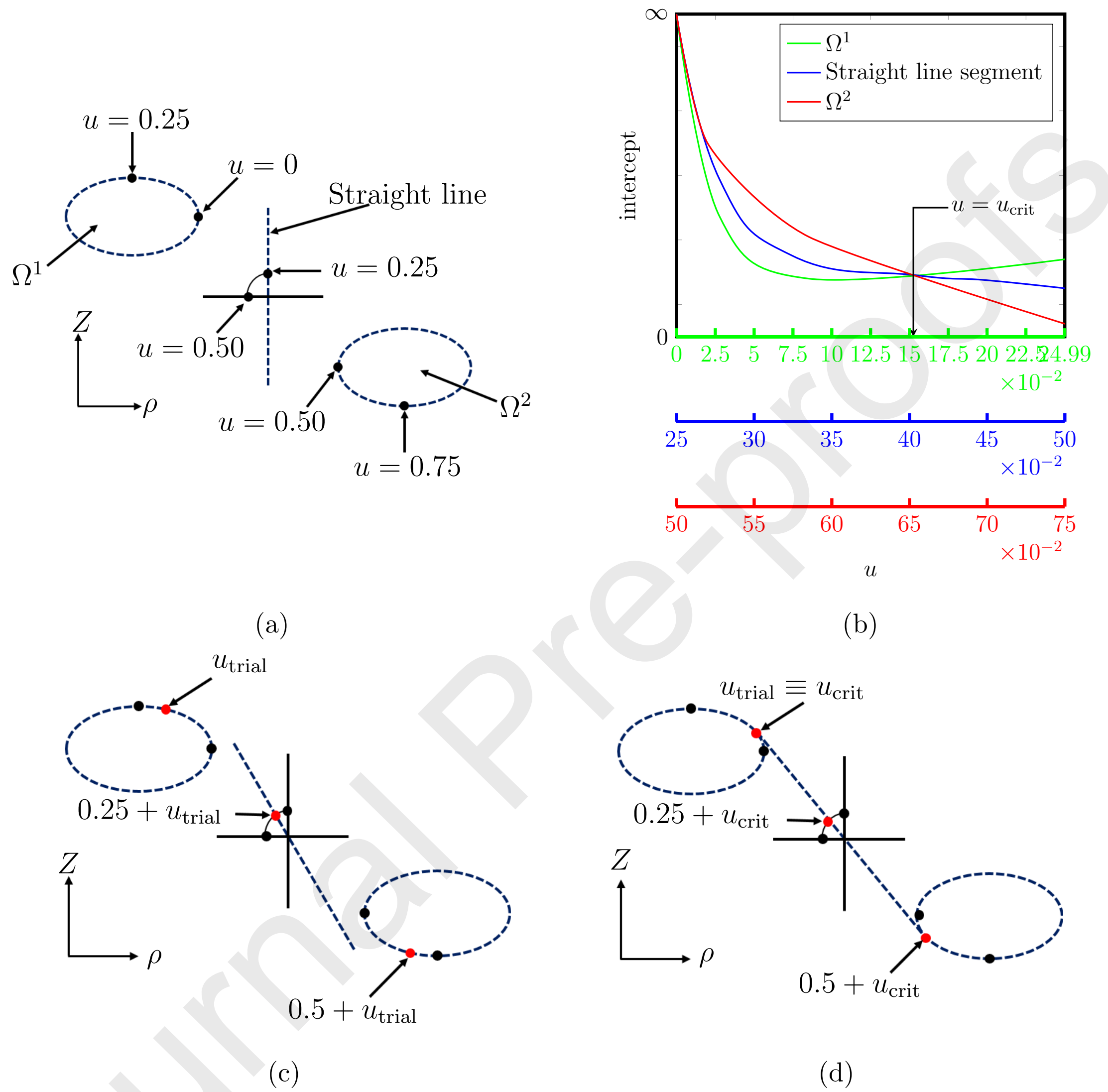

Figure 8: Illustration of the numerical method required to enforce C^1 continuity along a yarn's path between adjacent supporting contours and their adjoining straight line segment: (a) definition of parameters within a given crimp interval along a yarn's path, (b) numerical search for the critical parameter value u_{crit} between the straight line segment and its two adjoining supporting contours, (c) numerical search for tangency between a straight line segment and two adjacent supporting contours; note that $\Delta_{\text{line}} \neq \Omega^{1\prime}\big|_{u=u_{\text{trial}}} \equiv \Omega^{2\prime}\big|_{u=0.50+u_{\text{trial}}}$ but $\alpha_{\text{line}} \neq \alpha_{\Omega^1}|_{u=u_{\text{trial}}} \neq \alpha_{\Omega^2}|_{u=0.50+u_{\text{trial}}}$, and (d) numerical search for tangency between a straight line segment and two adjacent supporting contours; note that $\Delta_{\text{line}} \equiv \Omega^{1\prime}\big|_{u=u_{\text{crit}}} \equiv \Omega^{2\prime}\big|_{u=0.50+u_{\text{crit}}}$ and $\alpha_{\text{line}} \equiv \alpha_{\Omega^1}|_{u=u_{\text{crit}}} \equiv \alpha_{\Omega^2}|_{u=0.50+u_{\text{crit}}}$.

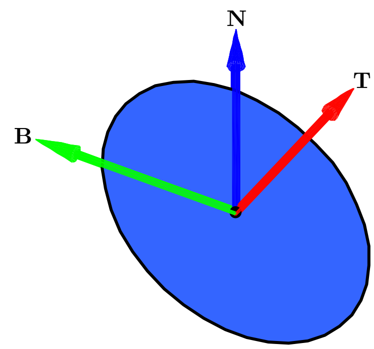

Figure 9: Local cross section of a yarn affixed to the **NB** plane of the $\{\mathbf{N}, \mathbf{B}, \mathbf{T}\}$ orthonormal basis.

noobed[2] fabrics [46, 47]. In these cases, the 'up-vector' may be defined such that it runs horizontally leftwards: a side-vector so to say. Nevertheless, there is no restriction on the directionality of these, so long as they are not parallel to the yarn's tangent vector.

Having defined the unit normal and bi-normal basis vectors in the local reference frame, the parametric surface of the entire yarn in the global reference frame becomes [48]

$$\mathbf{Q}(u,t) = \mathbf{S}(t) + (C(u)_x \hat{\mathbf{N}}(t) + C(u)_y \hat{\mathbf{B}}(t)) \quad \text{for } u \in [0,1] \quad \text{and} \quad t \in [0,1]. \tag{13}$$

Essentially, the local reference frame unit vectors morph the cross section from its initial configuration to its localised configuration. The left-hand term, $\mathbf{S}(t)$, translates the morphed cross section to the local point along the yarn path for which it is defined. For a given value of t, the outline of the yarn's localised surface can be traced, and the resulting vectors stored in an array. This process may continue until the yarn is completely traversed. Eventually, each successive surface outline may be connected using polygons to fully define the yarn's surface; the smoothness of the ensuing yarn is dictated by the frequency of sampling along its trajectory (see Figure 10).

4. Input data for generating a computational textile

The accuracy of computational models is dependent on the geometric parameters of the virtual domain. These geometric parameters pertain to the individual yarns (called yarn parameters) that comprise the textile, as well as the collective interaction of yarn parameters within the textile (called preform parameters) [40]. Yarn parameters include, fibre volume fraction, density, width, height and area. Preform parameters include, overall fibre volume fraction of textile, volume fraction and inter-yarn spacing of weft-wise and warp-wise yarns, areal density, height, width and thickness of preform. Both yarn and preform parameters can be sub-categorised into three [49]: (1) Input design parameters, (2) Measurable structural parameters, and (3) Interim calculated parameters. Tables 1 and 2 outline specifics of representative yarn and preform parameters, respectively. These yarn and preform parameters are also dependent on the type of textile being considered,

[2]Noobing is a term coined from the description of a special set of fabrics: Non-interlacing Orientating Orthogonally Binding fabrics. It has many synonyms in the literature, namely; 3D orthogonal weave, XYZ fabric, zero-crimp fabric polar fabric, and DOS (Directionally Oriented Structures).

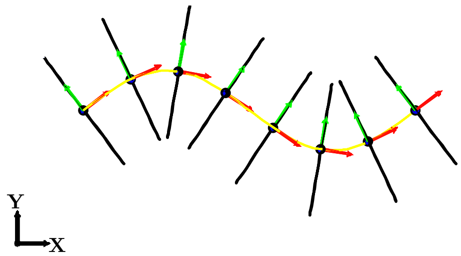

(a) **XY** view of local orthonormal basis vectors along yarn.

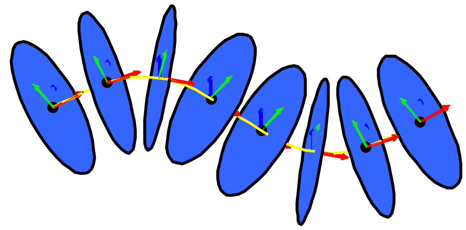

(b) View of local cross-sections along a yarn's path conformed to the $\{\mathbf{N}, \mathbf{B}, \mathbf{T}\}$ basis.

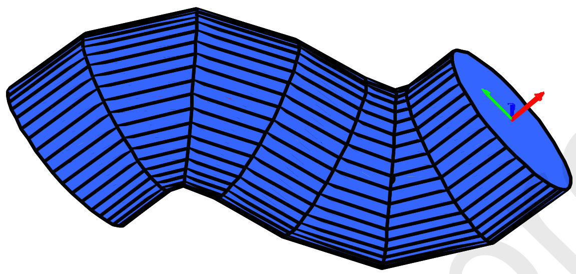

(c) View of fully defined yarn obtained from adjoining successive local cross sections as shown in b with polygons.

Figure 10: Sequence of steps required to define a yarn along an arbitrary curve. Notice the finesse of the yarn discretisation is chiefly dependent on the number of sampled cross sections along the yarn's path.

however, the method delineated earlier for defining yarn paths is general and, therefore, places no restrictions on the type of preform that can be analysed.

In generating representative virtual domains for textile composites, the underlying assumption is that the entire input design parameters and measurable structural parameters, for each textile, have been determined a priori, and supplied as inputs to the geometric modelling algorithm, TextCompGen. Hence, in principle, these primary data suffice as inputs for TextCompGen. For brevity and completeness, a simplified version of a flowchart for TextCompGen is shown in Figure 11. TextCompGen generates textiles with simple, pre-defined, geometric parameters: input design parameters and measurable parameters.

5. Physical properties of numerical textiles

TextCompGen generates textiles with simple, pre-defined, geometric parameters: input design parameters and measurable parameters. Nevertheless, important measurable structural parameters such as the packing factor in yarns, and volume proportion of yarns are required for proper numerical modelling of textiles; therefore, these parameters also need to be determined by TextCompGen. Incorporating the generated textiles, however, in finite element platforms, such as ABAQUS, requires additional geometric input data for adequate modelling to those supplied during the geometric generated phase. These

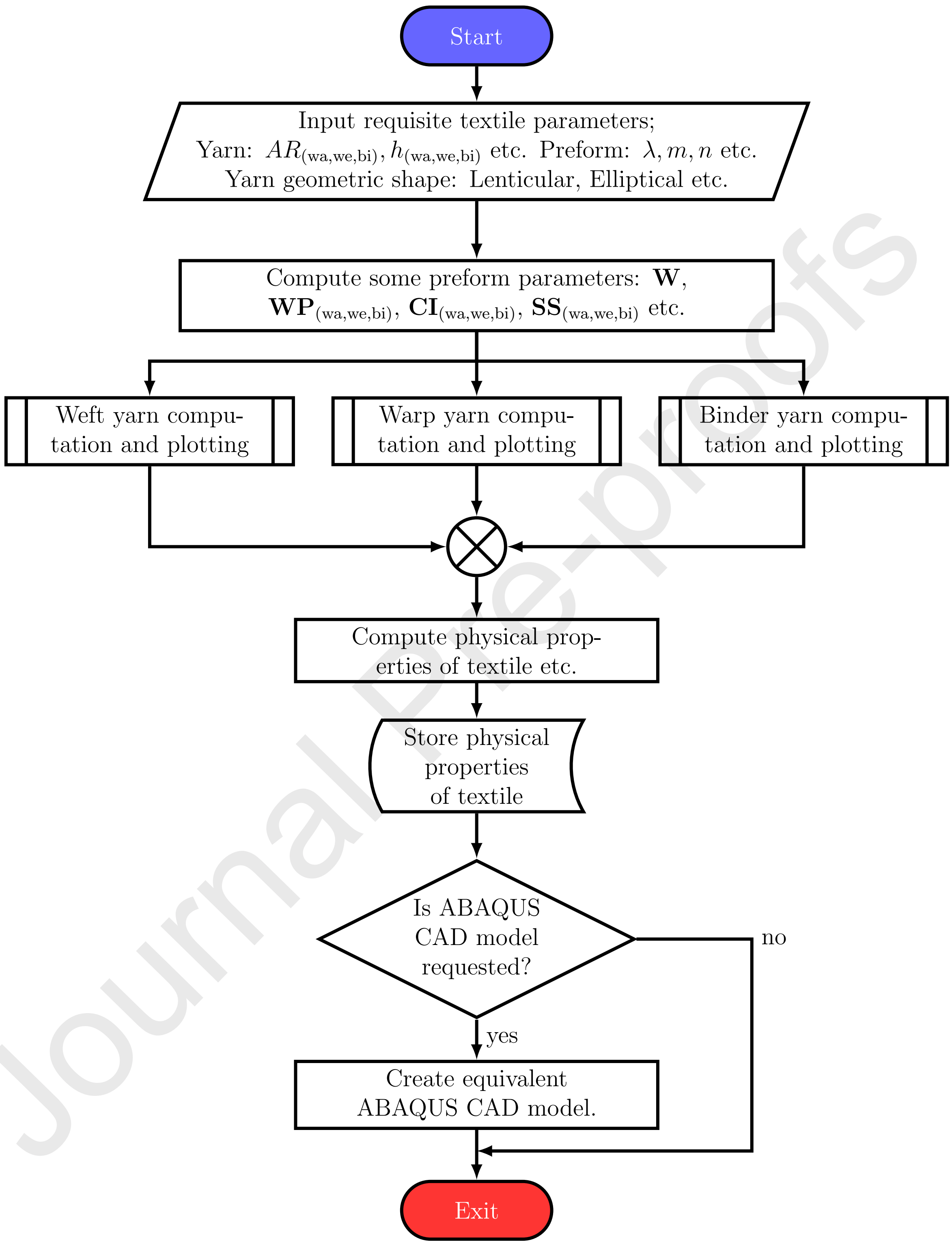

Figure 11: Flowchart for the geometric modelling algorithm, TextCompGen.

Table 1: Representative physical yarn parameters, reproduced from [49, 40].

Input design parameters	
T_{wa}, T_{we}, T_{bi}	Yarn count of warp, weft and binder yarns (Tex =g/km)
ρ_{wa}, ρ_{we}, ρ_{bi}	Density of warp, weft and binder yarns (g/km^3)
Measurable structural parameters	
β_{wa}, β_{we}, β_{bi}	Yarn packing factor for warp, weft and binder yarns
h_{wa}, h_{we}, h_{bi}	Height of warp, weft and binder yarns (cm)
w_{wa}, w_{we}, w_{bi}	Width of warp, weft and binder yarns (cm)
Interim calculated parameters	
A_{wa}, A_{we}, A_{bi}	Cross-sectional area of warp, weft and binder yarns (cm^2)
AR_{wa}, AR_{we}, AR_{bi}	Aspect ratio ($AR = w/h$) of warp, weft and binder yarns (g/km)

parameters are the interim calculated parameters. These parameters also have yarn-specific and preform-specific definitions as in Tables 1 and 2. As these parameters are only inferred, and not supplied, during the geometric modelling phase, TextCompGen computes them and supplies the data along with the geometric model to the finite element platform. The approach adopted for determining these parameters are discussed in this section.

5.1. Yarn fibre volume fraction

Meso-scale modelling approaches for textile composites, as used here, approximates yarns as solid volumes. These yarns are, however, composites that contain a mixture of fibres and matrix regions. Since the behaviour a each yarn is homogenized, a description of the volume proportion of the fibres and matrix composition within each yarn is required. The packing factor, β, is an index that measures the volume fraction of fibres within yarns. Consider Figure 12 which shows the cross section of a representative yarn with different packing arrangements of fibres.

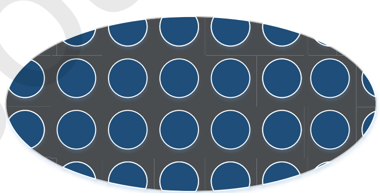

(a) Rectangular packing array

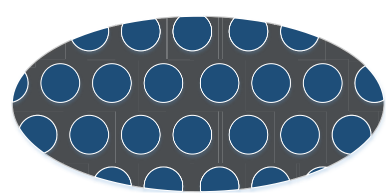

(b) Hexagonal packing array

Figure 12: Schematic of typical fibre packing arrangements for yarns.

The packing factor (or volume fraction) may be considered as a ratio between the cross-sectional area of the yarn and the total area of fibres enclosed within the region bounded

Table 2: Representative physical preform parameters, reproduced from [49, 40].

Input design parameters	
λ	Number of weft yarns that a binder yarn passes around in the weft layer before a reversal of direction
m	Ratio of warp yarns per layer to the total number of binder yarns within the preform
n	Number of warp layers
Measurable structural parameters	
P_{wa}	Ends/cm per warp layer along weft direction
P_{we}	Picks/cm per weft layer along warp direction
s	Spacing between adjacent yarns in the weft layer(cm)
ξ	Ratio of spacing between adjacent yarns to the corresponding yarn width in weft layer (s/w_{we})
H	Preform thickness
Interim calculated parameters	
o-V_f	Overall fibre volume fraction of preform/composite
D_a	Areal density (g/mm^2)
V_f^{wa}, V_f^{we}, V_f^{bi}	Volume fraction of warp, weft, and binder yarns

by this cross section given by

$$V_i^f = \frac{NA_{\mathrm{fibre}}}{A_i} \quad (i = \mathrm{wa}, \mathrm{we}, \mathrm{bi})\,, \tag{14}$$

where, N is the number of fibres within the cross section and A_{fibre} is the area of each fibre. Fibres generally have a circular cross sectional shape, therefore, their total area is given by

$$A_{\mathrm{fibre}} = \frac{\pi D_{\mathrm{fibre}}^2}{4}\,,$$

where D_{fibre} is the diameter of each fibre. For any of the arrangements depicted in Figure 12, a theoretical limit of the maximum possible packing factor exists for contiguously arranged fibres [50]. Alternative definitions of fibre volume fraction exist, such as using the relationship between the mass and density of the fibres, together with the total volume of the yarn [19].

For a positively oriented [3] smooth curve enclosing a non-hollow region defining a yarn's cross section, the cross-sectional area of this region is determined by

$$A_i = -\int_0^1 C(u)_y \, C'(u)_x \; \mathrm{d}u \quad (i = \mathrm{wa}, \mathrm{we}, \mathrm{bi}) \; , \tag{15}$$

where Green's theorem [51] has been applied (see **??**) and κ represents the unique geometric tag assigned to each yarn. It may be difficult, or even impossible, to obtain an explicit integral in elementary form using Equation (15): especially for the power ellipse formulation (i.e., Equation (4)) when the shape parameter is not equal to unity. In these cases, numerical quadrature approximation techniques become necessary [52, 53].

5.2. Yarn volume

The volume of individual yarns is another important material parameter which determines the overall mechanical properties of textiles. Due to the arbitrariness of determining a yarn's trajectory and associated cross-sectional area, a method for deducing the overall volume of each yarn is required.

Consider a yarn volume, V, enclosed by a boundary surface, $\mathbf{Q}^{\mathrm{abs}}$. Furthermore, let $\mathbf{Q}^{\mathrm{abs}}$ be defined such that $\mathbf{Q}^{\mathrm{abs}} = \mathbf{Q}(t,u) \cup \mathbf{S}_\alpha \cup \mathbf{S}_\beta$, where $\mathbf{Q}(t,u)$ represents the periphery of the entire yarn and $\mathbf{S}_i$, $(i = \alpha, \beta)$ represents the terminal end cap surfaces of the yarn that completely enclose the region, V. The volume of the region V enclosed by $\mathbf{Q}^{\mathrm{abs}}$ is

$$V_i = \int_0^1 \int_0^1 \mathbf{Q}_y \left(\frac{\partial \mathbf{Q}}{\partial t, x} \frac{\partial \mathbf{Q}}{\partial u, z} - \frac{\partial \mathbf{Q}}{\partial t, z} \frac{\partial \mathbf{Q}}{\partial u, x} \right) \mathrm{d}\,t\,\mathrm{d}\,u \; + \iint\limits_{S_\alpha} \mathbf{S}_{\alpha,y} \cdot \mathbf{n}_\alpha \, \mathrm{d}\mathbf{S}_\alpha \; + \iint\limits_{S_\beta} \mathbf{S}_{\beta,y} \cdot \mathbf{n}_\beta \, \mathrm{d}\mathbf{S}_\beta \tag{16}$$

where the Gauss-Ostrogradsky divergence theorem has been invoked [51]. The term $\mathbf{Q}_y$ is a vector-valued function $\mathbf{Q}_y = (0, y, 0)$ which satisfies the requirement that $\Delta \mathbf{Q}_y = 1$ based on the Gauss-Ostrogradsky divergence theorem. It is noted that other alternative vector-valued functions such as $\mathbf{Q}_x = (x, 0, 0)$ or $\mathbf{Q}_z = (0, 0, z)$ are also admissible in Equation (16); however, the terms within the equation have to be re-written for consistency and correctness. The shorthand i for $i \in \{x, y, z\}$ represents the laboratory basis component of the respective vector, and $\mathbf{n}_\alpha$ and $\mathbf{n}_\beta$ represent the unit outward normals or the terminal end caps. In practice, analytical solutions to Equation (16) can be challenging to obtain and numerical approximates of yarn volumes become necessary.

As an alternative, given a yarn of constant cross-sectional area, A_i, the volume of the yarn, V_i, is given by

$$V_i = A_i R_i \, , \quad (i = \mathrm{wa}, \mathrm{we}, \mathrm{bi}) \tag{17}$$

where, A_i is the cross-sectional area of the yarn, R_i arc length of the yarn's path given by

$$R_i = \int_{t_0}^{t_{n+5}} |\nabla \mathbf{S}\,(t)| \; \mathrm{d}t \qquad \text{for } t \in [0, 1]. \tag{18}$$

[3] The curve is traced out in an anticlockwise direction.

The arc length is sometimes referred to as a *rectified curved* because it determines the length of an irregular curve when it is stretched to form a straight line.

5.3. Yarn volume proportion

The volume proportion of yarn measures the volumetric composition of yarn types (i.e., warp-wise and weft-wise yarns) within a textile preform. Volume proportion, as opposed to volume fraction, has been used here to obviate possible instances of confusion with fibre volume fraction described in Section 5.1. The volume proportion of yarns, V_i^p , within a given textile is expressed as

$$V_i^p = \frac{\sum V_i}{V_{\text{preform}}} \quad (i = \text{wa}, \text{we}, \text{bi}) \,,$$

where V_{preform} represents the volume of the textile preform (see Section 5.5).

5.4. Yarn crimp factor

Crimp, or yarn undulation, is a measure the quantifies the straightness of a yarn in a given textile. It is a critical material property which influences the overall behaviour of textile and therefore requires quantification. There is no universal definition of crimp within both textile and composite industries and several definitions, therefore, exist [54]. A common definition of crimp in the textile industry is given by [20]

$$\text{Crimp}_i = \frac{R_i}{\text{wave length}} \,, \quad (i = \text{wa}, \text{we}, \text{bi}). \tag{19}$$

Similarly, a common definition of crimp within the composite industry, known as *crimp ratio* (CR), is given by

$$\text{CR}_i = \frac{\text{yarn amplitude}}{\text{wave length}} \,, \quad (i = \text{wa}, \text{we}, \text{bi}). \tag{20}$$

Figure 13 shows illustrations of the parameters defined in Equation (19) and Equation (20).

For all textile architectures, including non-planar weaving patterns of binder yarns [11], Equation (19) yields one definition of crimp for yarns. Conversely, the definition of crimp ratio in Equation (20) may yield several definitions per yarn, depending on yarn weaving architecture which makes it more cumbersome. Therefore, within TextCompGen, only the definition of crimp given by Equation (19) is used.

5.5. Preform volume

The volume of a textile preform is determined by the geometric parameters defining the individual yarns which comprise it. The volume of a perform is

$$V_{\text{preform}} = L_{\text{preform}} \, W_{\text{preform}} \, H_{\text{preform}} \tag{21}$$

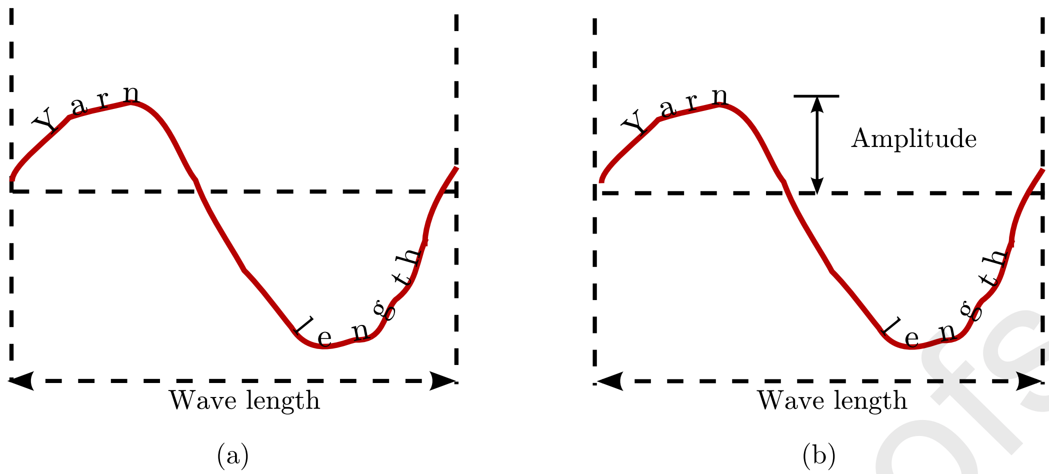

Figure 13: Illustration of two common crimp definitions: (a) Variables defined in Equation (19) and (b) Variables defined in Equation (20).

where L_{preform}, W_{preform} and H_{preform} represent the length, width and height of the fabric, respectively.

6. Generating geometric textile domains: an example

The idealised geometry of the selected textile architecture chosen for demonstrating the generation process of numerical fabrics, using the method discussed in this work, is shown in Figure 14. This textile is a through-the-thickness angle-interlock (AIC) woven architecture with low crimp [55]. This architecture was chosen because the entire geometric modelling input parameters required by TextCompGen for the fabric were reported and obtained from experimental micrograph analysis. Furthermore, other important physical preform properties such the overall fibre volume fraction (o-V_f) and the inter-yarn fibre volume fraction (iy-V_f) of the warp-wise and weft-wise yarns were also experimentally deduced. The reported geometric and physical parameters of the fabric are reported in Table 3. The objective of the computational example is two-fold: (1) to delineate the algorithmic representation of a woven textile topology, and (2) more important, to compare the computational and experimental fabric parameters, where applicable.

The virtual geometry adopted for predictive mechanical characterisation of textile composites is instrumental in determining the resulting accuracy. Previous researchers have concluded that a significant limitation of predictive models stems from the use of idealised geometries [56, 3]. Geometrically, consolidated woven textile composites have intricate architectures. During weaving and subsequent consolidation, yarns are interlaced, stretched and compacted. Furthermore, yarns are arbitrarily shaped locally due to inter-yarn and mould interactions. Therefore, it is infeasible to capture all the geometric features emanating from these nuances in computational models [37]; therefore, TextCompGen was designed to capture the principal features of the textile being studied. The principal features which ensure correspondence between the actual textile and geometric model are overall fibre volume fraction, o-V_f, and fabric thickness, H [35]. In addition, unlike typical idealised textile geometric models (see Figure 14), the binder yarns in actual con-

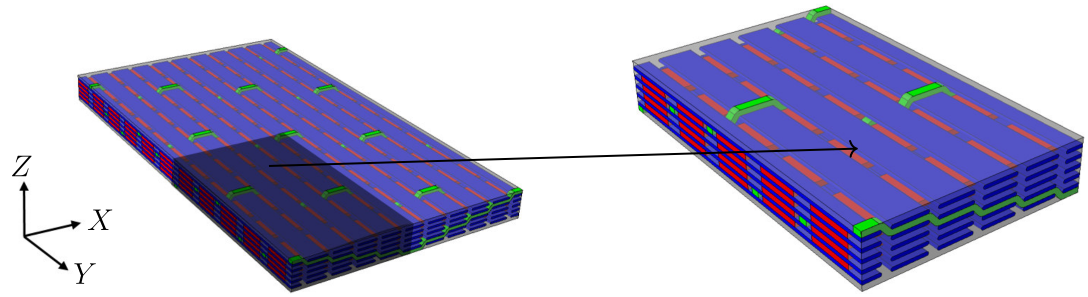

(a) (b)

Figure 14: Idealised geometry of a through-the-thickness angle interlock textile composite: (a) isometric view a unit cell, and (b) idealised view with five warp and weft yarns, and six binder yarns.

solidated fabrics are usually flush with weft yarns on the surface of the fabric along the thickness direction, as shown in Figure 15. This flush representation is achieved by enforcing maximum crimp of the surface weft yarns at crossover regions between the binder and weft yarns. This within TextCompGen two textile geometric models were generated: (1) models without flushed binder yarns, and (2) models with flushed binder yarns maximum crimp of the surface weft yarns was enforced at the crossover regions between the binder and weft yarns to maintain the experimentally derived fabric thickness.

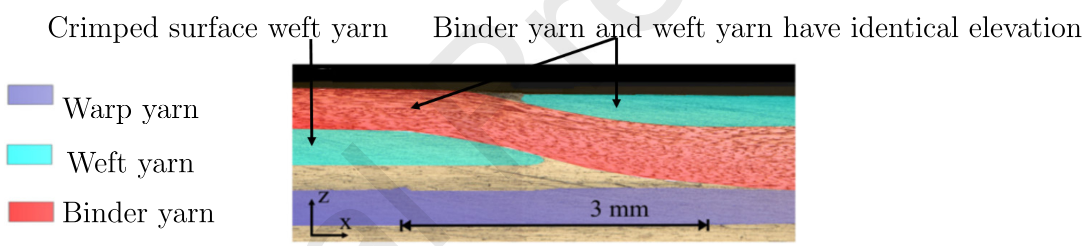

Figure 15: Micrograph image representing flushed surface of a typical woven angle interlock composite [57].

Consider the truncated AIC fabric shown in Figure 14b. The textile contains five levels of weft yarns and 4 levels of warp yarns and one level of binder yarns (i.e., $RL_{\mathrm{we}} = RL_{\mathrm{z,we}} = 5$, $RL_{\mathrm{wa}} = RL_{\mathrm{z,wa}} = 4$, $RL_{\mathrm{bi}} = RL_{\mathrm{z,bi}} = 1$). The truncated unit cell covers six crossovers along X and eleven crossovers along Y directions, respectively (i.e., $RC_{\mathrm{x}} = 6$, $RC_{\mathrm{x}} = 11$).

The weaving vector, $\mathbf{W}$, for the warp-wise yarns is given by

$$\mathbf{W} = \begin{bmatrix} \{6,5,4,3,2,1\} & \varnothing & \varnothing & \varnothing & \varnothing \\ \{2,2,2,2,2,2\} & \{3,3,3,3,3,3\} & \{4,4,4,4,4,4\} & \{5,5,5,5,5,5\} & \varnothing \\ \{3,2,1,2,3,4\} & \varnothing & \varnothing & \varnothing & \varnothing \\ \{2,2,2,2,2,2\} & \{3,3,3,3,3,3\} & \{4,4,4,4,4,4\} & \{5,5,5,5,5,5\} & \varnothing \\ \{2,3,4,5,6,5\} & \varnothing & \varnothing & \varnothing & \varnothing \\ \{2,2,2,2,2,2\} & \{3,3,3,3,3,3\} & \{4,4,4,4,4,4\} & \{5,5,5,5,5,5\} & \varnothing \\ \{5,6,5,4,3,2\} & \varnothing & \varnothing & \varnothing & \varnothing \\ \{2,2,2,2,2,2\} & \{3,3,3,3,3,3\} & \{4,4,4,4,4,4\} & \{5,5,5,5,5,5\} & \varnothing \\ \{4,3,2,1,2,3\} & \varnothing & \varnothing & \varnothing & \varnothing \\ \{2,2,2,2,2,2\} & \{3,3,3,3,3,3\} & \{4,4,4,4,4,4\} & \{5,5,5,5,5,5\} & \varnothing \\ \{1,2,3,4,5,6\} & \varnothing & \varnothing & \varnothing & \varnothing \end{bmatrix}. \tag{22}$$

The weave pitch vectors $\mathbf{WP}_{\mathrm{we}}$, $\mathbf{WP}_{\mathrm{wa}}$ and $\mathbf{WP}_{\mathrm{bi}}$ are given by

$$\mathbf{WP}_{\mathrm{we}} = \begin{bmatrix} \frac{w_{\mathrm{we}}}{2} & 3.265 & 3.265 & \dots & \dots & 3.265 \\ \frac{w_{\mathrm{we}}}{2} & 3.265 & 3.265 & \dots & \dots & 3.265 \\ \vdots & \vdots & \vdots & \vdots & \vdots & \vdots \\ \vdots & \vdots & \vdots & \vdots & \vdots & \vdots \\ \frac{w_{\mathrm{we}}}{2} & 3.265 & 3.265 & \dots & \dots & 3.265 \end{bmatrix}, \tag{23}$$

$$\mathbf{WP}_{\mathrm{wa}} = \begin{bmatrix} \frac{w_{\mathrm{wa}}}{2} + S_{\mathrm{bi}} & 5.2 & \dots & \dots & 5.2 \\ \vdots & \vdots & \vdots & \vdots & \vdots \\ \vdots & \vdots & \vdots & \vdots & \vdots \\ \frac{w_{\mathrm{wa}}}{2} + S_{\mathrm{bi}} & 5.2 & \dots & \dots & 5.2 \end{bmatrix}, \tag{24}$$

$$\mathbf{WP}_{\mathrm{bi}} = \left[\frac{w_{\mathrm{wa}}}{2} + \frac{w_{\mathrm{bi}}}{2} + \frac{S_{\mathrm{bi}}}{2}, 5.2, \cdots, \cdots, \cdots, 5.2\right], \tag{25}$$

where S_{bi} is the average in-plane binder spacing. Using the arguments from Equation (7), the crimp interval and support structure matrix matrices $\mathbf{CI}_{\mathrm{i}}$ and $\mathbf{SS}_{\mathrm{i}}$, respectively, for

$i \in \{\mathrm{we}, \mathrm{wa}, \mathrm{bi}\}$ are given by

$$\mathbf{CI}_{\mathrm{wa}} = \begin{array}{rc} & \begin{array}{ccccc} L_1^1, L_1^2, L_2^1, L_2^2, L_3^1, L_3^2, L_4^1, L_4^2, L_5^1, L_5^2 & \cdots & \cdots & \cdots & \cdots \end{array} \\ \begin{array}{r} C_{\mathrm{y}} = 2, C_{\mathrm{y}} = 4, \cdots, C_{\mathrm{y}} = 10 \\ \vdots \\ \vdots \\ \vdots \end{array} & \left[\begin{array}{ccccc} \{1,1,1,1,1,1,1,1,1,1\} & \cdots & \cdots & \cdots & \cdots \\ \{2,2,2,2,2,2,2,2,2,2\} & \cdots & \cdots & \cdots & \cdots \\ \{3,3,3,3,3,3,3,3,3,3\} & \cdots & \cdots & \cdots & \cdots \\ \{4,4,4,4,4,4,4,4,4,4\} & \cdots & \cdots & \cdots & \cdots \end{array}\right] \end{array}, \tag{26}$$

$$\mathbf{SS}_{\mathrm{wa}} = \begin{array}{rc} & \begin{array}{ccccc} L_1^1, L_1^2, L_2^1, L_2^2, L_3^1, L_3^2, L_4^1, L_4^2, L_5^1, L_5^2 & \cdots & \cdots & \cdots & \cdots \end{array} \\ \begin{array}{r} C_{\mathrm{y}} = 2, C_{\mathrm{y}} = 4, \cdots, C_{\mathrm{y}} = 10 \\ \vdots \\ \vdots \\ \vdots \end{array} & \left[\begin{array}{ccccc} \{+,+,+,+,+,+,+,+,+,+\} & \cdots & \cdots & \cdots & \cdots \\ \{+,+,+,+,+,+,+,+,+,+\} & \cdots & \cdots & \cdots & \cdots \\ \{+,+,+,+,+,+,+,+,+,+\} & \cdots & \cdots & \cdots & \cdots \\ \{-,-,-,-,-,-,-,-,-,-\} & \cdots & \cdots & \cdots & \cdots \end{array}\right] \end{array}, \tag{27}$$

$$\mathbf{CI}_{\mathrm{bi}} = \begin{array}{rc} & L_1^1, L_1^2, L_2^1, L_2^2, L_3^1, L_3^2, L_4^1, L_4^2, L_5^1, L_5^2 \\ \begin{array}{r} C_{\mathrm{y}} = 1 \\ C_{\mathrm{y}} = 3 \\ C_{\mathrm{y}} = 5 \\ C_{\mathrm{y}} = 7 \\ C_{\mathrm{y}} = 9 \\ C_{\mathrm{y}} = 11 \end{array} & \left[\begin{array}{c} \{5,5,4,4,3,3,2,2,1,1\} \\ \{2,2,1,1,1,1,2,2,3,3\} \\ \{2,2,3,3,4,4,5,5,5,5\} \\ \{5,5,5,5,4,4,3,3,2,2\} \\ \{3,3,2,2,1,1,1,1,2,2\} \\ \{1,1,2,2,3,3,4,4,5,5\} \end{array}\right] \end{array}, \tag{28}$$

$$\mathbf{SS}_{\mathrm{bi}} = \begin{array}{rc} & L_1^1, L_1^2, L_2^1, L_2^2, L_3^1, L_3^2, L_4^1, L_4^2, L_5^1, L_5^2 \\ \begin{array}{r} C_{\mathrm{y}} = 1 \\ C_{\mathrm{y}} = 3 \\ C_{\mathrm{y}} = 5 \\ C_{\mathrm{y}} = 7 \\ C_{\mathrm{y}} = 9 \\ C_{\mathrm{y}} = 11 \end{array} & \left[\begin{array}{c} \{+,-,+,-,+,-,+,-,+,-\} \\ \{+,-,+,-,-,+,-,+,-,+\} \\ \{-,+,-,+,-,+,-,+,+,-\} \\ \{-,+,+,-,+,-,+,-,+,-\} \\ \{+,-,+,-,+,-,-,+,-,+\} \\ \{-,+,-,+,-,+,-,+,-,+\} \end{array}\right] \end{array}, \tag{29}$$

$$\mathbf{CI}_{\mathrm{we}} = \begin{array}{r} \\ C_{\mathrm{x}}=1, C_{\mathrm{x}}=2, \cdots, C_{\mathrm{y}}=5 \\ \vdots \\ \vdots \\ \vdots \\ \vdots \end{array} \begin{array}{c} \begin{array}{ccccc} L_1^1, L_1^2, L_2^1, L_2^2, L_3^1, L_3^2 & \cdots & \cdots & \cdots & \cdots \end{array} \\ \left[\begin{array}{ccccc} \{11,7,7,7,7,7,7\} & \cdots & \cdots & \cdots & \cdots \\ \{8,11,8,8,8,8,8\} & \cdots & \cdots & \cdots & \cdots \\ \{9,9,9,9,11,9\} & \cdots & \cdots & \cdots & \cdots \\ \{11,7,7,7,7,7,7\} & \cdots & \cdots & \cdots & \cdots \\ \{11,4,4,4,4,4\} & \cdots & \cdots & \cdots & \cdots \end{array} \right] \end{array}, \tag{30}$$

$$\mathbf{SS}_{\mathrm{we}} = \begin{array}{r} \\ C_{\mathrm{x}}=1, C_{\mathrm{x}}=2, \cdots, C_{\mathrm{y}}=5 \\ \vdots \\ \vdots \\ \vdots \\ \vdots \end{array} \begin{array}{c} \begin{array}{ccccc} L_1^1, L_1^2, L_2^1, L_2^2, L_3^1, L_3^2 & \cdots & \cdots & \cdots & \cdots \end{array} \\ \left[\begin{array}{ccccc} \{+,-,-,-,-,-\} & \cdots & \cdots & \cdots & \cdots \\ \{-,-,-,-,-,-\} & \cdots & \cdots & \cdots & \cdots \\ \{-,-,-,-,-,-\} & \cdots & \cdots & \cdots & \cdots \\ \{+,+,+,+,+,+\} & \cdots & \cdots & \cdots & \cdots \\ \{-,+,+,+,+,+\} & \cdots & \cdots & \cdots & \cdots \end{array} \right] \end{array}. \tag{31}$$

With respect to individual properties of yarns comprising the fabric, only the cross-sectional areas were specified for each yarn type (i.e., warp, weft and binder yarn) as reported in Table 3. In TextCompGen, this data was stored for individual yarns in the yarn type vectors $\mathbf{YT}_{\mathrm{i}}$ for $i \in \{\mathrm{we}, \mathrm{wa}, \mathrm{bi}\}$ using a pre-defined unique reference number.

Figure 16 illustrates the differences between a consolidated AIC fabric generated by TextCompGen with flushed and unflushed surface weft yarns. Table 4 compares data from these computational analogues of the AIC fabric generated by TextCompGen and experiments. Predictions yielded by the computational model with flushed surface binder yarns are within 3 % of experimentally derived values. This is in contrast to the unflushed computational model which has a 35 % discrepancy when compared with experimental data. In both geometric cases, flushed and unflushed, it was difficult to match the experimentally observed iy-V_f and the geometrically determined iy-V_f to yield the appropriate o-V_f. This difficulty is well-known in literature [35]; thus, it is common practice in geometric modelling to alter iy-V_f to achieve the desired o-V_f. Therefore, the iy-V_f was increased for both cases by approximately 2 % and 22 %, respectively, in order to match the experimental o-V_f. The increase was satisfactory for the flushed fabric because the maximum adjusted iy-V_f was 68.3 % which is sufficiently below the acceptable experimental maximum threshold of 75 %. In contrast, the increase of iy-V_f for the unflushed fabric is unacceptable because the adjusted value exceeds the 75 % threshold appreciably. Furthermore, in terms of mechanical modelling, the unflushed model contains excess matrix pockets on the fabric's surfaces. These spurious pockets can lead to exaggerated localised deformations, particularly in cases where strain rate dependence is assessed.

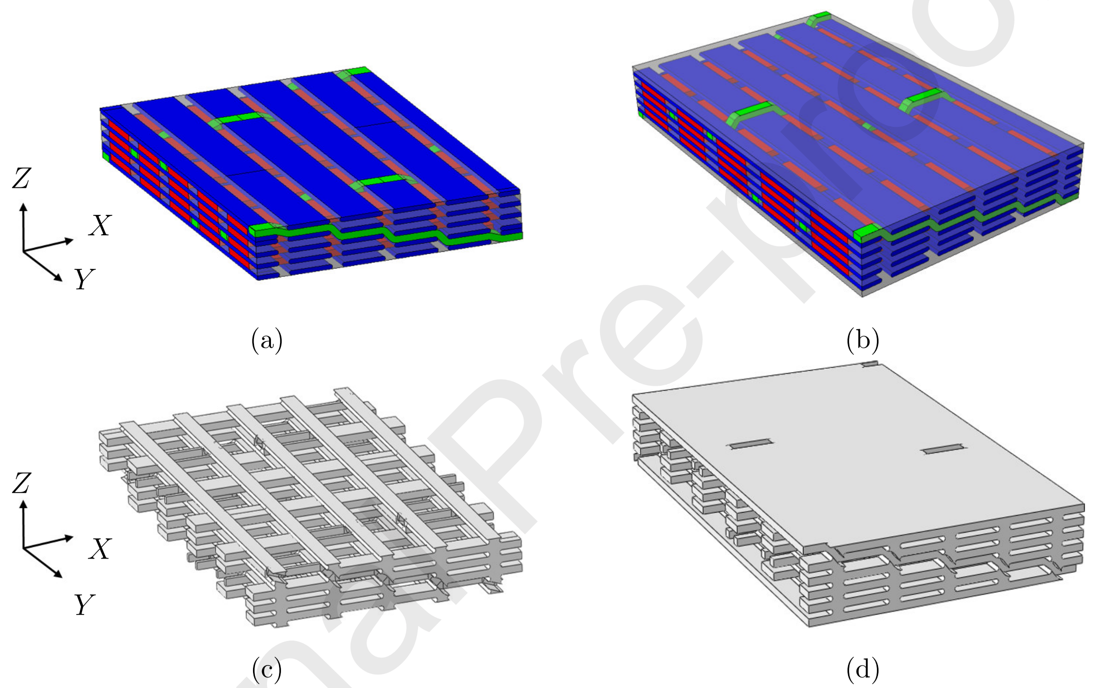

Figure 16: Comparison between a consolidated AIC fabric generated by TextCompGen with flushed and unflushed surface weft yarns: (a) fabric with flushed surface weft yarns, (b) fabric without flushed surface weft yarns, (c) matrix pockets of a, and (c) matrix pockets of b.

Table 3: Experimentally deduced parameters for the test AIC architecture [58].

Parameter	Value
Yarn parameters	
AR_{wa}, AR_{bi}, AR_{we}	8.54, 1.52, 9.67
w_{wa}, w_{bi}, w_{we} (mm)	3.5, 0.625, 2.65
iy-V_f^{wa}, iy-V_f^{bi}, iy-V_f^{we} (%)	64.4, 66.3, 63.6
V_f^{wa}, V_f^{bi}, V_f^{we} (%)	64.4, 66.3, 63.6
Warp, Binder and Weft cross-sectional shape	[ ], [ ], ( )
Preform parameters	
Thickness, H (mm)	3
Overall fibre volume fraction, o-V_f (%)	51
λ	5
m	1:1
n	4
P_{wa} (mm^{-1})	0.446
P_{we} (mm^{-1})	0.315
s (mm)	0.615
ξ	0.232

Table 4: Comparison between the geometric feature of the actual AIC fabric and the computationally-generated AIC fabric.

	Actual textile	Computational textile			
Parameter		unflushed	error (%)	flushed	error (%)
H (mm)	3	3.83	26.58	3.01	0.33
iy-V_f^{warp} (%)	64.4	86.4	34.16	66.4	3.1
V_f^{warp} (%)	-	49.04	-	48.5	-
iy-V_f^{weft} (%)	63.6	85.6	34.59	65.6	3.1
V_f^{weft} (%)	-	48.30	-	47.2	-
iy-V_f^{binder} (%)	66.3	88.3	33.18	68.3	2.9
V_f^{binder} (%)	-	2.66	-	4.3	-
o-V_f (%)	51	51	0	51	0
ρ^{areal} (g/m^2)	-	5388	-	4389	-
Warp cross-sectional shape	[ ]	[ ]		[ ]	
Weft cross-sectional shape	( )	[ ]		[ ]	
Binder cross-sectional shape	( )	[ ]		[ ]	
Surface weft yarn crimp	moderate	extreme		extreme	

7. Computational examples of woven textiles

In this section, simple computational examples of woven textile composites generated by TextCompGen are shown.

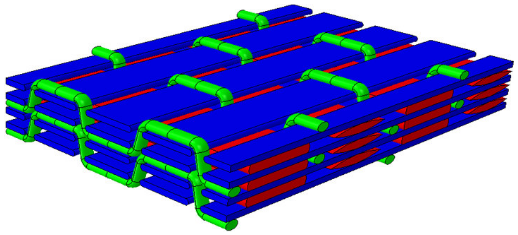

(a) Layer-to-layer orthogonal interlock architecture

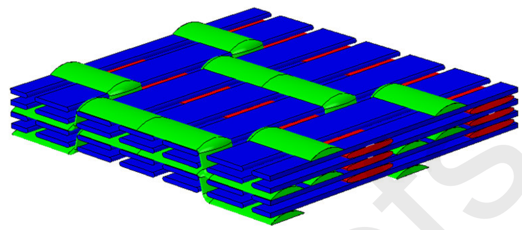

(b) Layer-to-layer angle interlock architecture

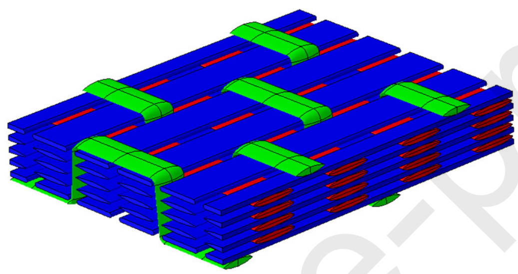

(c) Through-thickness orthogonal interlock architecture

Figure 17: Computational examples of typical woven textile architectures generated by TextCompGen.

8. Conclusion

Generating computational analogues of textiles requires three key elements: (1) definition of the fabric's topology, (2) definition of individual yarn paths, and (3) definition of cross-sectional shapes which enclose fibres contained within each yarn.

A fabric's topology is defined by decomposing its architecture into simplified crossover and non-crossover regions. Furthermore, the architecture is streamlined into in-plane and out-of-plane arrangements of yarns. This decomposition allows individual yarns and layers to be easily identified for a given fabric. Yarn paths are decomposed into a series of *crimp intervals* which represent the in-plane path of a yarn as it traverses from one crossover region to the next. The path of a yarn within each crimp interval is further decomposed into two curves and one straight line segment. The curves emanate from the mutual interaction between the yarn of interest and adjacent yarns which support it at crossover regions, using a notion of *supporting contours*. The straight line segment represents the path of the yarn that extends between two adjacent crossover regions. The straight line segment and supporting contours are joined such that at least C^1 is enforced. Several different shape functions such as *ellipse*, *power-ellipse*, and *lenticular* shape functions, were used to describe localised cross-sectional geometry of yarns, as its path is traversed. These shape functions contain *shape parameters* which enable them describe a plethora of cross-sectional shapes. To completely describe the volume of a yarn, the yarn's path and cross-sectional shape functions were unified through the use of a local, right-handed orthonormal unit basis vectors $\{\hat{\mathbf{N}}, \hat{\mathbf{B}}, \hat{\mathbf{T}}\}$ to *morph* the cross-sections to remain normal to the local yarn's tangent as it is traversed.

A comparison between data from computational geometric models and experiments showed that models designed with flushed binder yarns on fabric surfaces yields results which are within 3 % of experiments. This is in contrast to computational models with unflushed surfaces which produced results with 35 % discrepancy.

References

[1] M. I. Okereke, A. I. Akpoyomare, M. S. Bingley, Virtual testing of advanced composites, cellular materials and biomaterials: A review, Composites Part B: Engineering 637–662doi:10.1016/j.compositesb.2014.01.007.

[2] A. R. R. Melro, P. P. P. Camanho, S. T. T. Pinho, Influence of geometrical parameters on the elastic response of unidirectional composite materials, Composite Structures (11) 3223–3231. doi:10.1016/j.compstruct.2012.05.004.

[3] C. Chapman, J. Whitcomb, Effect of Assumed Tow Architecture on Predicted Moduli and Stresses in Plain Weave Composites, Journal of Composite Materials 29 (16) (1995) 2134–2159. doi:10.1177/002199839502901603.

[4] M. I. Okereke, A. I. Akpoyomare, A virtual framework for prediction of full-field elastic response of unidirectional composites, Computational Materials Science (null) 82–99. doi:10.1016/j.commatsci.2012.12.036.

[5] L. Mishnaevsky, Three-dimensional numerical testing of microstructures of particle reinforced composites, Acta Materialia (14) 4177–4188. doi:10.1016/j.actamat.2004.05.032.

[6] L. T. Harper, C. Qian, T. A. Turner, S. Li, N. A. Warrior, Representative volume elements for discontinuous carbon fibre composites Part 1: Boundary conditions, Composites Science and Technology (2) 225–234. doi:10.1016/j.compscitech.2011.11.006.

[7] S. V. Lomov, G. Perie, D. S. Ivanov, I. Verpoest, D. Marsal, Modeling three-dimensional fabrics and three-dimensional reinforced composites: challenges and solutions, Textile Research Journal (1) 28–41. doi:10.1177/0040517510385169.

[8] F. Robitaille, B. R. Clayton, A. C. Long, B. J. Souter, C. D. Rudd, Geometric modelling of industrial preforms: Warp-knitted textiles, Proceedings of the Institution of Mechanical Engineers, Part L: Journal of Materials Design and Applications (2) 71–90. doi:10.1177/146442070021400203.

[9] F. Robitaille, B. R. Clayton, A. C. Long, B. J. Souter, C. D. Rudd, Geometric modelling of industrial preforms: Woven and braided textiles, Proceedings of the Institution of Mechanical Engineers, Part L: Journal of Materials Design and Applications (2) 69–83. doi:10.1177/146442079921300201.

[10] G. Hivet, A. Wendling, V. Salle, B. Laine, P. Boisse, Modeling strategies for fabrics unit cell geometry application to permeability simulations, International Journal of Mater Form 3 (2010) 727–730. doi:10.1007/s12289-010-087.

[11] F. Stig, S. Hallström, Spatial modelling of 3D-woven textiles, Composite Structures (5) 1495–1502. doi:10.1016/j.compstruct.2011.12.003.

[12] S. V. Lomov, G. Huysmans, I. Verpoest, Hierarchy of Textile Structures and Architecture of Fabric Geometric Models, Textile Research Journal (6) 534–543. doi:10.1177/004051750107100611.

[13] G. Hivet, P. Boisse, Consistent 3D geometrical model of fabric elementary cell. Application to a meshing preprocessor for 3D finite element analysis, Finite Elements in Analysis and Design (1) 25–49. doi:10.1016/j.finel.2005.05.001.

[14] Y. Wang, X. Sun, Digital-element simulation of textile processes, Composites Science and Technology 61 (2001) 311–319.

[15] Y. Miao, E. Zhou, Y. Wang, B. a. Cheeseman, Mechanics of textile composites: Micro-geometry, Composites Science and Technology (7-8) 1671–1678. doi:10.1016/j.compscitech.2008.02.018.

[16] Y. Wang, Y. Miao, D. Swenson, B. A. Cheeseman, C.-F. Yen, B. LaMattina, Digital element approach for simulating impact and penetration of textiles, International Journal of Impact Engineering (5) 552–560. doi:10.1016/j.ijimpeng.2009.10.009.

[17] D. Durville, Simulation of the mechanical behaviour of woven fabrics at the scale of fibers, International Journal of Material Forming (S2) 1241–1251. doi:10.1007/s12289-009-0674-7.

[18] J. F. Ganghoffer, F. Pastrone (Eds.), Mechanics of Microstructured Solids: Cellular Materials, Fibre Reinforced Solids and Soft Tissues, Vol. 46, Springer, 2009.

[19] M. Sherburn, Geometric and Mechanical Modelling of Textiles, Ph.d, The University of Nottingham (2007).

[20] F. T. Peirce, The Geometry of Cloth Structure, Journal of the Textile Institute Transactions (3) T45–T96. doi:10.1080/19447023708658809.

[21] A. Kemp, An Extension of Peirce's Cloth Geometry to the Treatment of Non-circular Threads, Journal of the Textile Institute Transactions (1) T44–T48. doi:10.1080/19447025808660119.

[22] C. G. Provatidis, S. G. Vassiliadis, On the performance of the geometrical models of fabrics for use in computational mechanical analysis, International Journal of Clothing Science and Technology (5) 434–444. doi:10.1108/09556220410554624.

[23] F. Robitaille, A. C. Long, I. A. Jones, C. D. Rudd, Automatically generated geometric descriptions of textile and composite unit cells, Composites Part A: Applied Science and Manufacturing (4) 303–312. doi:10.1016/S1359-835X(03)00063-0.

[24] S. V. Lomov, A. V. Gusakov, G. Huysmans, A. Prodromou, I. Verpoest, Textile geometry preprocessor for meso-mechanical models of woven composites, Composites Science and Technology (11) 2083–2095.

[25] S. V. Lomov, G. Huysmans, Y. Luo, R. S. Parnas, A. Prodromou, I. Verpoest, F. R. Phelan, Textile composites: modelling strategies, Composites Part A: Applied Science and Manufacturing 1379–1394.

[26] M. Sherburn, a. Long, a. Jones, J. Crookston, L. Brown, Prediction of textile geometry using an energy minimization approach, Journal of Industrial Textiles (4) 345–369. doi:10.1177/1528083711420747.

[27] Y. Mahadik, S. R. Hallett, Finite element modelling of tow geometry in 3D woven fabrics, Composites Part A: Applied Science and Manufacturing (9) 1192–1200. doi:10.1016/j.compositesa.2010.05.001.

[28] R. B. Turan, A. Okur, Variation of the yarn cross-section in fabric, Textile Research Journal (7) 719–724. doi:10.1177/0040517511435009.

[29] S. V. Lomov, I. Verpoest, T. Peeters, D. Roose, M. Zako, Nesting in textile laminates: geometrical modelling of the laminate, Composites Science and Technology (7) 993–1007. doi:10.1016/S0266-3538(02)00318-4.

[30] R. D. Hale, M. Villa, Influence of Opposing Wave Nesting in Compression-loaded Composites, Journal of Composite Materials 37 (13) (2003) 1149–1166. doi:10.1177/002199803033447.

[31] S. V. Lomov, Composite Reinforcements for Optimum Performance, Elsevier. doi:10.1533/9780857093714.2.200.

[32] M. Blacklock, H. Bale, M. Begley, B. Cox, Generating virtual textile composite specimens using statistical data from micro-computed tomography: 1D tow representations for the Binary Model, Journal of the Mechanics and Physics of Solids (3) 451–470. doi:10.1016/j.jmps.2011.11.010.

[33] A. C. Long, S. V. Lomov, I. Verpoest, F. Robitaille, P. Boisse, P. Harrison, M. Clifford, W. R. Yu, J. Dominy, C. D. Rudd, M. D. Wakeman, J. A. E. Manson, A. Gokce, S. G. Advani, I. A. Jones, A. K. Pickett, A. R. Horrocks, B. K. Kandola, J. Lowe, J. G. Ellis, K. van de Velde, Design and manufacture of textile composites, Woodhead and CRC Press, 2005.

[34] G. Hivet, P. Boisse, Consistent mesoscopic mechanical behaviour model for woven composite reinforcements in biaxial tension, Composites Part B: Engineering (2) 345–361. doi:10.1016/j.compositesb.2007.01.011.

[35] D. S. Ivanov, S. V. Lomov, 2 - Modelling the structure and behaviour of 2D and 3D woven composites used in aerospace applications, in: P. E. Irving, C. Soutis (Eds.), Polymer Composites in the Aerospace Industry, Woodhead Publishing, pp. 21–52. doi:http://dx.doi.org/10.1016/B978-0-85709-523-7.00002-5.

[36] S. D. Green, A. C. Long, B. S. F. El Said, S. R. Hallett, Numerical modelling of 3D woven preform deformations, Composite Structures 747–756doi:10.1016/j.compstruct.2013.10.015.

[37] S. D. Green, M. Y. Matveev, A. C. Long, D. Ivanov, S. R. Hallett, Mechanical modelling of 3D woven composites considering realistic unit cell geometry, Composite Structures 284–293doi:10.1016/j.compstruct.2014.07.005.

[38] R. Gerlach, C. R. Siviour, J. Wiegand, N. Petrinic, In-plane and through-thickness properties, failure modes, damage and delamination in 3D woven carbon fibre composites subjected to impact loading, Composites Science and Technologydoi:10.1016/j.compscitech.2011.11.032.

[39] R. G. Rinaldi, M. Blacklock, H. Bale, M. R. Begley, B. N. Cox, Generating virtual textile composite specimens using statistical data from micro-computed tomography: 3D tow representations, Journal of the Mechanics and Physics of Solids (8) 1561–1581. doi:10.1016/j.jmps.2012.02.008.

[40] M. Ansar, W. Xinwei, Z. Chouwei, Modeling strategies of 3D woven composites: A review, Composite Structures (8) 1947–1963. doi:10.1016/j.compstruct.2011.03.010.

[41] W. J. Shanahan, J. W. S. Hearle, An energy method for calculations in fabric mechanics part II: examples of application of the method to woven fabrics, Journal of the Textile Institute (4) 92–100. doi:10.1080/00405007808631426.

[42] C. C. Wong, A. C. Long, M. Sherburn, F. Robitaille, P. Harrison, C. D. Rudd, Comparisons of novel and efficient approaches for permeability prediction based on the fabric architecture, Composites Part A: Applied Science and Manufacturing (6) 847–857. doi:10.1016/j.compositesa.2005.01.020.

[43] S. V. Lomov, D. Ivanov, I. Verpoest, M. Zako, T. Kurashiki, H. Nakai, S. Hirosawa, Meso-FE modelling of textile composites: Road map, data flow and algorithms, Composites Science and Technology (9) 1870–1891. doi:10.1016/j.compscitech.2006.10.017.

[44] E. Abbena, S. Salamon, A. Gray, Modern Differential Geometry of Curves and Surfaces with Mathematica,, 3rd Edition, Textbooks in Mathematics, Taylor & Francis.

[45] G. Farin, Curves and Surfaces for Computer Aided Geometric Design: a Practical Guide, third edit Edition, Vol. i, Academic Press Limited, San Diego, CA, 1993.

[46] F. Stig, 3D-woven Reinforcement in Composites, Ph.D. thesis, KTH School of Engineering Sciences (2012).

[47] N. Khokar, 3D-Weaving: Theory and Practice, Journal of the Textile Institute (2) 193–207. doi:10.1080/00405000108659570.

[48] S. Adanur, T. Liao, 3D modeling of textile composite preforms, Composites Part B: Engineering (6) 787–793. doi:10.1016/S1359-8368(98)00036-5.

[49] Z. Wu, Three-dimensional exact modeling of geometric and mechanical properties of woven composites, Acta Mechanica Solida Sinica (5) 479–486. doi:10.1016/S0894-9166(09)60299-8.

[50] R. F. Gibson, Principles of composite material mechanics, 2nd Edition, no. 205, CRC, Boca Raton.

[51] R. Larson, B. Edwards, Calculus: Early Transcendental Functions, Cengage Learning.

[52] E. Kreyszig, Advanced Engineering Mathematics, John Wiley & Sons, Limited.

[53] R. Burden, D. Faires, Numerical analysis, Thomson Brooks/Cole, Belmont, CA, 2005.

[54] E. Alexander, M. Lewin, H. V. Muhsam, M. Shiloh, Definition and Measurement of Crimp of Textile Fibers, Textile Research Journal (8) 606–617. doi:10.1177/004051755602600804.

[55] R. Gerlach, C. R. Siviour, J. Wiegand, N. Petrinic, In-plane and through-thickness properties, failure modes, damage and delamination in 3D woven carbon fibre composites subjected to impact loading, Composites Science and Technology (3) 397–411. doi:10.1016/j.compscitech.2011.11.032.

[56] S. R. Hallett, B. G. Green, W.-G. Jiang, K. H. Cheung, M. R. Wisnom, The open hole tensile test: a challenge for virtual testing of composites, International Journal of Fracture (2) 169–181. doi:10.1007/s10704-009-9333-8.

[57] R. Gerlach, Characterisation of the strain rate dependent behaviour of 3D composites using a hierarchical approach, Ph.D. thesis, University of Oxford (2010).

[58] R. Gerlach, C. R. Siviour, N. Petrinic, J. Wiegand, Experimental characterisation and constitutive modelling of RTM-6 resin under impact loading, Polymer (11) 2728–2737. doi:10.1016/j.polymer.2008.04.018.